Published in final edited form as:

Cell Rep. 2023 August 29; 42(8): 112805. doi:10.1016/j.celrep.2023.112805.

MEF2A suppresses stress responses that trigger DDX41-dependent IFN production

Julian R. Smith[1], **Jack W. Dowling**[2], **Matthew I. McFadden**[2,3], **Andrew Karp**[2,4], **Johannes Schwerk**[1], **Joshua J. Woodward**[5], **Ram Savan**[1], **Adriana Forero**[2,6,7,8,*]

[1]Department of Immunology, University of Washington, Seattle, WA 98109, USA

[2]Department of Microbial Infection and Immunity, College of Medicine, The Ohio State University, Columbus, OH 43210, USA

[3]Biomedical Sciences Graduate Program, The Ohio State University, Columbus, OH 43210, USA

[4]Discovery PREP, The Ohio State University, Columbus, OH 43210, USA

[5]Department of Microbiology, University of Washington, Seattle, WA 98109, USA

[6]Cancer Biology Program, Comprehensive Cancer Center, The Ohio State University, Columbus, OH 43210, USA

[7]Infectious Diseases Institute, The Ohio State University, Columbus, OH 43210, USA

[8]Lead contact

SUMMARY

Cellular stress in the form of disrupted transcription, loss of organelle integrity, or damage to nucleic acids can elicit inflammatory responses by activating signaling cascades canonically tasked with controlling pathogen infections. These stressors must be kept in check to prevent unscheduled activation of interferon, which contributes to autoinflammation. This study examines the role of the transcription factor myocyte enhancing factor 2A (MEF2A) in setting the threshold of transcriptional stress responses to prevent R-loop accumulation. Increases in R-loops lead to the induction of interferon and inflammatory responses in a DEAD-box helicase 41 (DDX41)-, cyclic GMP-AMP synthase (cGAS)-, and stimulator of interferon genes (STING)-dependent manner. The loss of MEF2A results in the activation of ATM and RAD3-related (ATR) kinase, which is also necessary for the activation of STING. This study identifies the role of MEF2A in sustaining transcriptional homeostasis and highlights the role of ATR in positively regulating R-loop-associated inflammatory responses.

*Correspondence: adriana.forero@osumc.edu.

AUTHOR CONTRIBUTIONS

Investigation and formal analysis, J.R.S., J.W.D., M.I.M., A.K., J.S., and A.F.; conceptualization, J.R.S., J.W.D., and A.F.; writing, J.R.S. and A.F.; methodology, J.W.; supervision, R.S. and A.F.; funding acquisition, R.S. and A.F.

DECLARATION OF INTERESTS

These authors declare no competing interests.

SUPPLEMENTAL INFORMATION

Supplemental information can be found online at https://doi.org/10.1016/j.celrep.2023.112805.

In brief

Smith et al. show that depletion of the transcription factor MEF2A leads to R-loop accumulation and DDX41-/cGAS-/STING-dependent inflammatory responses. ATR kinase activity is required to activate STING-dependent inflammation.

Graphical Abstract

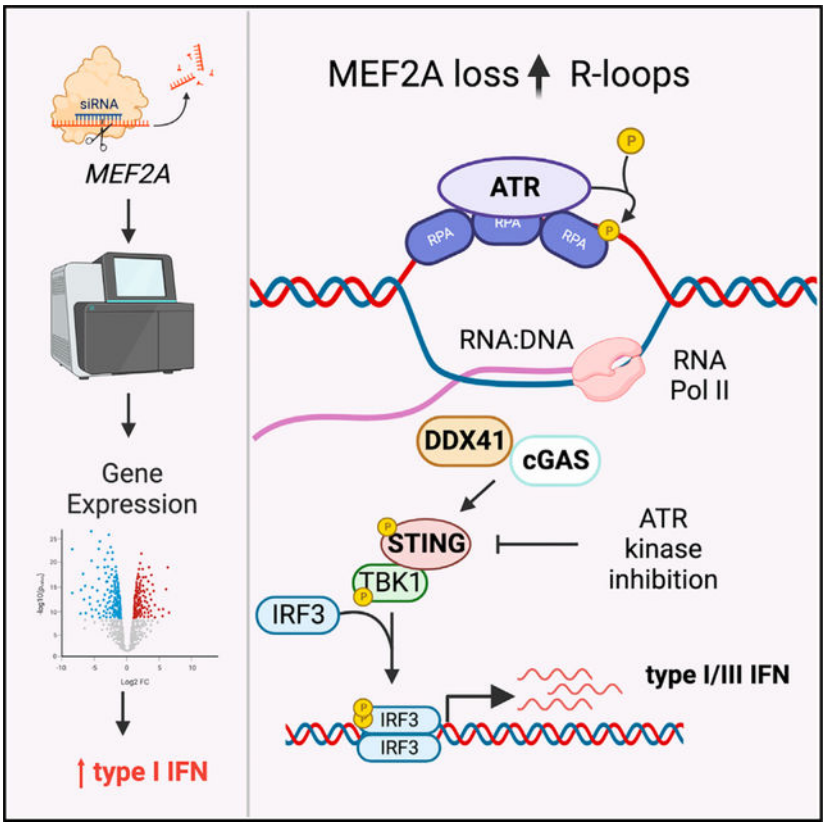

INTRODUCTION

The detection of nucleic acids or DNA breaks by pattern recognition receptors (PRRs) promotes the formation of signalosomes that recruit Tank-binding kinase 1 (TBK1) to phosphorylate transcription factors such as interferon regulatory factor 3 (IRF3). Phosphorylation of C-terminal serine residues of IRF3 allow for its dimerization and translocation to the nucleus, where it transactivates type I interferon (IFNα/β) and type III IFN (IFNλ) gene expression. IFNs activate signal transducer and activator of transcription (STAT) to form the transcriptionally active complex ISGF3 and drive IFN-stimulated gene (ISG) expression.[1] ISGs are critical effectors of the antiviral immune response and regulate various cellular processes to inhibit cell proliferation and promote inflammation. While the regulation of IFN responses is best characterized in the context of viral infection, accumulation and mislocalization of self-nucleic acids or the loss of nuclear genome integrity can also drive noxious sterile IFN-mediated inflammation. These latter processes are the hallmark of autoinflammatory pathologies known as interferonopathies.[2] Thus, it is

critical to define the factors that protect organelle and genomic integrity, thereby preventing the unscheduled or excessive inflammation.

The major nucleic acid-sensing pathways induced by the accumulation of mis-localized or damaged DNA converge on the adaptor molecule, stimulator of interferon genes (STING). Three nucleic acid sensors have been characterized as upstream regulators of STING: cyclic GMP-AMP synthase (cGAS), IFNγ inducible factor 16 (IFI16), and DEAD-box helicase 41 (DDX41). Accumulation of double-stranded DNA (dsDNA) activates cGAS-mediated synthesis of the second messenger, 2′,3′-cyclic GMP-AMP (cGAMP), which induces STING activation.[3,4] Genomic DNA breaks induce IFI16-dependent non-canonical pathways to drive cGAS-independent STING activation.[5] R-loops are RNA:DNA hybrid structures occurring naturally in ~5%–10% of the genome,[6] but their accumulation is associated with Aicardi-Goutières syndrome (AGS),[7] an autoinflammatory disorder driven by STING-mediated inflammation.[8] DEAD-box RNA helicases recognize these RNA:DNA structures to prevent their accumulation.[9,10] One such helicase, DDX41, activates STING after recognition of dsDNA[11–13] and RNA:DNA transcripts generated by retroviral infection.[14] Recent studies have shown that DDX41 is recruited to R-loops, promoting their resolution to prevent DNA damage.[15] However, a role, if any, for DDX41-dependent processes in the induction of IFN-mediated inflammation upon R-loop enrichment remains to be determined.

The DNA damage response (DDR) kinases Ataxia-telangiectasia mutated (ATM), ATM and RAD3-related (ATR), and DNA-dependent protein kinase catalytic subunit (DNA-PKcs) coordinate cell-cycle arrest and repair of DNA damage and host inflammatory responses associated with genotoxic stress,[16,17] cytosolic DNA accumulation,[18,19] and DNA virus infection.[20] Among these kinases, ATR is the central regulator of the replicative stress response (RSR) that occurs under conditions associated with stalled replication fork progression, such as nucleotide pool depletion, and R-loop accumulation. ATR phosphorylates substrates that mediate cell-cycle arrest to prevent chromosomal breaks[21,22] and promotes R-loop resolution and proper chromosome segregation.[23–25] While ATM and DNA-PKcs have been linked to IRF3 activation and IFN-driven inflammatory responses, the mechanisms by which ATR contributes to IFN production are less clear.

The myocyte enhancing factor 2 (MEF2) transcription factors, composed of 4 evolutionarily conserved proteins, MEF2A–D, have emerged as potential regulators of inflammation.[26–29] MEF2 proteins have important developmental[30] and homeostatic roles, as mice deficient in these factors display embryonic lethality or early post-natal lethality.[31,32] Our study focuses on MEF2A, the least characterized immune regulator in this family. MEF2A loss-of-function (LOF) mutations associate with an enhanced risk for adverse coronary artery disease outcomes, which could be exacerbated by aberrant IFN induction.[33] We show that acute depletion of MEF2A results in spontaneous IFN antiviral and inflammatory responses. We demonstrate that MEF2A expression prevents the induction of transcriptional stress and the accumulation of R-loops. This increase in RNA:DNA hybrid formation drives DDX41-/cGAS-/STING-mediated IFN responses and the activation of ATR. Lastly, we show that ATR kinase activity is required to support STING activation in this context. These findings

position MEF2A as a positive regulator of genomic stability that protects from unscheduled IFN-driven inflammation.

RESULTS

Loss of MEF2A leads to spontaneous IFN production and type I IFN-dependent inflammation

Given the potential connection between MEF2 proteins and inflammation, we examined the impact of one MEF2 family member on the transcriptional program in myocytes, a cellular target of inflammation caused by viral infections. As such, we used dicer substrate small interfering RNA (dsiRNA) to transiently deplete highly expressed MEF2 genes in the human cardiomyocyte cell line AC16. Transient depletion of *MEF2A* allowed us capture acute gene expression changes while circumventing possible functional compensation by other MEF2 paralogs, as previously described in knockout cells.[34] AC16 cells expressed high levels of *MEF2A* and *MEF2D*, moderate levels of *MEF2C*, and low levels of *MEF2B* mRNA (Figure 1A). This is consistent with the expression of MEF2 transcription factors in left ventricular adult human cardiomyocytes (GTEx database) (Figure S1A). Based on this, we independently targeted MEF2A, MEF2C, and MEF2D and measured changes in IFN induction. The depletion of *MEF2A* (Figure 1B, left) resulted in an increase in IFNB1 mRNA expression (Figure 1B, right). Neither the silencing of *MEF2C* nor *MEF2D* elicits significant changes in IFNB1 mRNA expression relative to control transfected cells (Figures 1B and 1C). To validate the reproducibility of *MEF2A* targeting in driving IFN induction, we tested two additional MEF2A-targeting siRNAs. We found that in all cases, *MEF2A* silencing led to the phosphorylation of the IFN responsive transcription factor STAT1 at tyrosine 701 (Y701) relative to control transfected cells (Figure S1B). Genome-wide transcriptional signatures captured by RNA sequencing revealed robust differentially expressed (DE) transcripts, in which 519 genes were significantly upregulated and 201 genes were significantly downregulated in *MEF2A*-targeted cells compared with cells transfected with non-targeting control (NC) dsiRNA (Figure 1D; Data S1). Gene Ontology analysis identified enriched biological functions among the upregulated genes following MEF2A depletion. We observed significant enrichment in pathways associated with innate immune inflammation and type I IFN responses among the upregulated genes (Figure 1E). This was consistent with an increase not only in *IFNB1* expression but also in the ISG *CXCL10* in MEF2A knockdown (KD) cells (Figure 1F). We recapitulated this phenotype in immortalized human fibroblasts, which have similar MEF2 gene expression profiles to myocytes (Figure S1C). Silencing of *MEF2A* was sufficient to induce both *IFNB1* mRNA and that of ISGs such as *CXCL10* (Figure S1D, left). Finally, we observed similar upregulation of *IFNB1* and *CXCL10* mRNA in human macrophage-like cells, THP-1, induced by the KD of *MEF2A* expression (Figure S1D, right). Together, these results suggest that MEF2A, but not other MEF2 protein family members, is a negative regulator of spurious type I IFN transcription across multiple human cell types.

Having observed an enrichment of genes involved in IFN responses, we addressed whether this was associated with increased resistance to viral infection. *MEF2A* silencing protects cells from to the cytolytic effects of vesicular stomatitis virus (VSV) infection compared

with control cells (Figure 2A). Similarly, loss of MEF2A conferred AC16 cells with protection against the cardiotropic enterovirus Coxsackievirus B3 (CVB3), which exhibited a 75% reduction in viral RNA accumulation relative to control cells (Figure 2B). Previously, we have demonstrated that such decreases in viral RNA correspond to a significant attenuation in infectious virus production.[35] These data suggest that MEF2A loss leads to the secretion of bioactive IFNs that can establish a cellular antiviral state.

Cell-intrinsic antiviral responses are coordinated by both type I and III IFNs. Both IFN families can promote the activation of ISGF3 to promote transcriptional induction of ISG expression.[36] As we observed both type I and III IFN gene mRNA induction after MEF2A depletion (Data S1), we asked whether the secretion of IFN drove MEF2A-dependent inflammatory responses. We engineered a Huh7 cell-based luciferase reporter assay to monitor ISGF3-mediated transcriptional activation in response to secreted IFN. Transfer of supernatants from *MEF2A* KD muscle cells led to a significant increase in luciferase activity relative to treatment with supernatants derived from control transfected cells (Figure 2C). Huh7 cells respond to exogenous type I and III IFN stimulation (Figure S2A). We examined whether human cardiomyocytes could respond to exogenous recombinant type I (IFNβ) and III (IFNλ3) IFN stimulation by measuring the induction of ISG mRNA. Treatment with recombinant IFNβ induced significant expression of *ISG15* and *CXCL10* mRNAs at 9 and 24 h post-stimulation (Figure 2D). In contrast, IFNλ3 stimulation did not induce the expression of either of these two ISGs (Figure 2D). We then confirmed the predominant inflammatory role for type I IFN by treating AC16 cells with the pan-type I IFN inhibitor B18R.[37] B18R pre-treatment decreased *ISG15* mRNA induction post-*MEF2A* silencing (Figure 2E). This was concomitant with decreased STAT1 phosphorylation (Y701) in B18R-treated cells relative to vehicle treatment (Figure 2F). IRF3 activation (serine 386 phosphorylation) was unaffected by B18R blockade of type I IFN signaling (Figure 2G), suggesting that decreases in MEF2A promote signaling transduction cascades upstream of IRF3 to drive IFN expression. Of note, levels of phosphorylated STAT1 induced by silencing of MEF2A were comparable to those induced by IFNβ stimulation, both of which enhanced IRF3 activation and increased IRF1 protein expression (Figure S2B). Exogenous expression of dsiRNA-resistant *MEF2A* (Figure S2C) suppressed IRF3 activation after targeting of endogenous *MEF2A* (Figures 2H and S2D), demonstrating the specificity of MEF2A in preventing spurious IFN responses. Together, these data suggest that IFN is secreted after MEF2A silencing and that the establishment of the antiviral state in cardiomyocytes depends solely on type I IFNs.

Inflammatory responses in MEF2A-depleted cells are STING dependent

To further define signaling mechanisms for IFN responses in the wake of MEF2A deficiency, we first confirmed that IRF3 was indispensable for this process. For this purpose, we generated *IRF3*-deficient cardiomyocytes using CRISPR-Cas9 genome editing technologies. Deletion of IRF3 abrogated the activation of STAT1 in response to *MEF2A* silencing (Figure 3A), suggesting minimal compensation from additional IRFs, such as IRF1 or IRF7, which can transactivate IFN genes[16,38,39] and are induced by MEF2A depletion (Figure S2B). IRF3 activation is mediated by RNA and DNA sensors and converge on adaptor molecules such as mitochondrial antiviral-signaling protein (MAVS) (RNA sensing)

and STING (DNA sensing).[40] We confirmed that both RNA- and DNA-sensing pathways were functional in our cellular model by measuring the induction of IFN (*IFNB1, IFNL1*) and ISG (*CXCL10*) mRNAs following the transfection of cells with either a specific RIG-I RNA agonist[41] or calf-thymus DNA[42] (Figure S3A). In addition, AC16 cells responded to TLR3 activation with poly(I:C) and infection with Sendai virus (SeV) (Figure S3B), which activate MAVS-dependent responses through RIG-I and MDA5.[43]

To discern which of these nucleic acid-sensing pathways is engaged in response to *MEF2A* silencing, we depleted either STING (*TMEM173*) or *MAVS* prior to targeting *MEF2A* expression. We found that STING, but not MAVS, was necessary to promote the activation and phosphorylation of TBK1 and IRF3 upstream of type I IFN induction. Similarly, we observed that STAT1 phosphorylation following *MEF2A* depletion (Figure 3B) was muted only in cells deficient for STING. Silencing of *MAVS* did not abrogate STAT1 phosphorylation relative to that observed in control cells (Figure 3B). We then generated STING knockout cells by targeting *TMEM173* using CRISPR-Cas9 genome editing (Figure 3C). In these cells, silencing of *MEF2A* (Figure S3C) did not promote the accumulation of IFNB1 mRNA that was observed in control (H1) cells (Figure 3C). Consistent with the previous results, *MEF2A* KD was sufficient to promote STING phosphorylation at serine 366, a prerequisite for IRF3 activation[44] (Figure 3E). Together, these data indicate that MEF2A promotes homeostatic functions that prevent STING activation and inhibit spontaneous IFN-mediated inflammation.

The loss of MEF2A compromises genomic integrity

Both the loss of nuclear DNA integrity and the accumulation of endoplasmic reticulum (ER) stress have been associated with pathogen-independent, STING-mediated inflammation.[45] To determine whether MEF2A is necessary to sustain either DNA integrity or ER function, we silenced MEF2A expression in AC16 cells and measured DNA damage or ER stress response markers. The loss of MEF2A led to an accumulation of phosphorylated histone 2AX (γH2A.X), a marker of DNA damage (Figure 3F). Similar γH2A.X increases were observed following treatment with the topoisomerase II inhibitor etoposide, known to elicit genotoxic stress (Figure 3F). However, neither the loss of *MEF2A* nor treatment with etoposide led to an accumulation of ATF4 or enhanced splicing of XBP1 (XBP1s), hallmarks of the ER stress response (Figure S3D). On the other hand, treatment with thapsigargin, a sarco/ER calcium ATPase (SERCA) inhibitor, led to expected increases in both ATF4 protein expression and XBP1 splicing. We conclude that loss of MEF2A results in the accumulation of γH2A.X and DNA damage, which activates STING and type I IFN induction.

The accrual of DNA breaks can result in an accumulation of extranuclear DNA in the form of micronuclei. Experimentally, inhibition of microtubule dynamics by treatment with nocodazole promotes the mis-segregation of chromosomes and accumulation of micronuclei (Figure 3G, right). We assessed whether the DDR associated with MEF2A KD was accompanied by accumulation of chromosomal aberrations by quantifying the percentage of cells with noticeable micronuclei (Figure 3G, left). Compared with NCs, depletion of MEF2A led to a significant increase in the percentage of cells containing micronuclei.

Thus, loss of MEF2A compromises genomic integrity, promoting cellular stress via the STING-IFN axis.

The accumulation of cytosolic nucleic acid or the loss of nuclear DNA compartmentalization is sensed by cGAS and results in the synthesis of 2′,3′-cGAMP. To assess if cGAS was required for IFN induction upon *MEF2A* silencing, we generated cGAS knockout (KO) cells by CRISPR-Cas9 genome editing. Functional ablation of *cGAS* was confirmed by measuring 2′,3′-cGAMP synthesis upon calf-thymus DNA transfection. Cells deficient in cGAS were impaired in 2′,3′-cGAMP synthesis, while there was detectable accumulation of cGAMP in wild-type (WT; H1) NC cells (Figure S3E). We depleted MEF2A in either H1 or *cGAS* KO cells and observed that both STING phosphorylation (Figure 3H) and IRF3 activation were dampened by cGAS deletion (Figure 3I). Because IFI16 can also mediate non-canonical induction of type I IFN responses in response to DNA breaks in a STING-dependent manner,[5] we generated IFI16 KO cells (Figure 3J). Unlike data from cGAS-deficient counterparts, IFI16 KO and control cells induced comparable levels of *IFNB1* mRNA upon MEF2A depletion (Figure 3K). We conclude that MEF2A expression is necessary to prevent accumulation of DDRs at steady state, which would drive IFN production in a cGAS-/STING-dependent, but IFI16-independent, pathway.

ATR kinase is pivotal for production of IFN following MEF2A depletion

The accumulation of DNA lesions activates DDRs coordinated by the kinases ATM, ATR, and DNA-PKcs to ultimately promote DNA repair.[23–25,46] In addition, DDR kinases have been implicated in the regulation of IFN following genotoxic stress.[5,16,18] Thus, we addressed whether DDR kinase activity was necessary for the induction of inflammation in response to cellular stress elicited by decreased MEF2A expression. We pre-treated human fibroblasts with selective inhibitors of ATR (ATRi, ETP46464), ATM (ATMi, KU-55933), or DNA-PKcs (DNA-PKi, NU7441) kinase activity 2 h prior to MEF2A depletion. Inhibition of ATR kinase activity specifically muted the activation of both IRF3 and STAT1 in response to the loss of MEF2A (Figure 4A). In contrast, robust IRF3 and downstream STAT1 phosphorylation was observed when cells were treated with ATM kinase inhibitors, as previously reported.[47] Inhibition of DNA-PK kinase activity led to a minimal increase in basal IRF3 and STAT1 phosphorylation but did not affect STAT1 activation in response to MEF2A KD (Figure 4A). In addition, we observed that decreased MEF2A expression enhanced S33 phosphorylation of the ATR substrate RPA32.[48] Pre-treatment of cells with a highly specific ATR kinase inhibitor (AZD6738) at non-cytotoxic doses (Figure S4A) led to a marked decrease in basal RPA32 S33 phosphorylation. ATR kinase inhibition also prevented increases in RPA32 S33 phosphorylation in response to MEF2A depletion (Figure 4C). Of note, RPA32 phosphorylation at S4/8, a substrate for ATM and DNA-PK, was not induced by MEF2A depletion. On the other hand, S4/8 phosphorylation was enhanced by ATR kinase inactivation. These data suggest that induction of MEF2A induces stress responses that drive ATR activation. In addition, it is possible that the resulting IFN induction is not induced by DDRs in this model.

We further defined the requirement for ATR kinase activity for IFN production in cardiac muscle cells using a fluorescent cell-based assay (AC16-ISRE-GFP) in which activation of

interferon-stimulated response element (ISRE)-mediated transcription drives the expression of green fluorescent protein (GFP).[49] As a primary control, IFN treatment of AC16-ISRE-GFP cells resulted in GFP increases, as did *MEF2A* silencing (Figures 4D and S4B). The increase in GFP expression elicited by *MEF2A* KD (Figure S4C, left) was not due to changes in cellular viability after transfection (Figure S4C, right). Pre-treatment of reporter cells with ATR kinase inhibitors muted the expression of GFP in response to the loss of MEF2A (Figure 4D). To test if activation of ATR in a MEF2A-independent context could stimulate IFN production, we treated cells with hydroxyurea (HU). HU depletes deoxynucleoside triphosphates (dNTPs) and activates ATR.[50] Low doses of HU induced ATR-dependent ISRE activity (Figure S4D) and STING phosphorylation in AC16 cells (Figure S4E). These data suggest a potentially conserved mechanism by which ATR kinase activation promotes IFN responses.

In this regard, we next assessed whether ATR kinase inhibition regulated the activation of STING in the context of MEF2A depletion. Treatment of AC16 cells with AZD6738 prior to siRNA transfection inhibited both STING and IRF3 phosphorylation upon the silencing of *MEF2A* (Figure 4E). This decrease in STING activation was not due to changes in the expression of DNA sensors (Figure S4G). As expected, the loss of STING and IRF3 activation was accompanied by a decrease in *IFNB1* mRNA induction (Figure 4F). This phenotype was recapitulated in fibroblasts. Inhibition of ATR kinase activity led to similarly decreased expression of type I IFN after MEF2A silencing relative to control transfected cells (Figure S4D). Interestingly, we found that ATR kinase inhibition did not affect the recognition of dsDNA ligands such as poly(deoxyadenylic-deoxythymidylic) acid (polydA:dT) (Figure S4H). Together, these data suggested that ATR kinase activity is necessary to drive the induction of inflammatory responses independent from dsDNA recognition.

MEF2A depletion promotes the accumulation of R-loops

ATR functions as a protector of the genome in the case of aberrant R-loop formation.[24] R-loops are triple-stranded nucleic acid structures that form during transcription as nascent RNA threads back into the template DNA strand and form an RNA:DNA hybrid.[51] The failure to resolve these structures can further result in replication fork stalling and renders the genome susceptible to DNA breaks.[52] To determine whether MEF2A loss impacted R-loop homeostasis, we probed the formation of RNA:DNA hybrids *in vitro* by assessing the cross-reactivity of genomic DNA isolated from *MEF2A*-depleted and control cells with S9.6, an antibody that recognizes RNA:DNA (Figure 5A). We observed an enhanced level of S9.6 antibody reactivity in nucleic acid MEF2A KD samples relative to control cells. Importantly, treatment with recombinant RNase H, which specifically degrades RNA:DNA hybrid strands, resulted in the near complete loss of S9.6 staining, further confirming an accumulation of R-loops in muscle cells lacking MEF2A. As an additional control, neither silencing of MEF2A nor treatment with RNase H affected dsDNA-specific antibody reactivity in any of the samples. Using an orthogonal approach, we conducted immunofluorescence-based assessment of R-loop accumulation in cells after KD of MEF2A using an antibody specific for RNA:DNA hybrids (S9.6) (Figure 5B). Overall, we observed a significant increase in the intensity of nuclear S9.6 foci in *MEF2A*-depleted cells relative to

NC cells (Figure 5C). RNASEH1 is a cell endogenous RNase that specifically targets RNA in RNA:DNA hybrids and thus functions to resolve cellular R-loops. We measured IFN production in cells in which we overexpressed RNASEH1 prior to targeting *MEF2A*. The levels of *IFNB1* mRNA induction (Figure 5D) were decreased in RNASEH1-overexpressing cells relative to vector-expressing cells (Figure 5E). Conversely, we observed synergistically enhanced *IFNB1* mRNA expression (Figure 5F) in cells in which we silenced both *RNASEH1* and *MEF2A* (Figure 5G). Taken together, our data indicate that the loss of MEF2A drives IFN responses due to R-loop accumulation, as their resolution restores immune homeostasis.

DDX41 is required for the induction of R-loop-mediated IFN responses

The accumulation of R-loops is known to drive inflammatory response due to cGAS/STING pathway activation.[11,14] The DEAD-box helicase DDX41 is recruited to R-loops to promote their resolution.[53–55] However, whether DDX41 promotes or prevents the inflammatory responses associated with R-loop accumulation has yet to be addressed. Accordingly, we generated DDX41-deficient cells by CRISPR-Cas9 genome editing and measured inflammatory responses upon MEF2A depletion. The phosphorylation of IRF3 and STAT1 was attenuated dramatically in DDX41-deficient cells relative to WT controls (Figure 6A). Consistent with these findings, *DDX41* KO cells showed decreased STING phosphorylation (Figure 6B) and a decreased induction of *IFNB1* mRNA following *MEF2A* silencing relative to WT controls (Figure 6C). Interestingly, DDX41 deficiency associated with a noticeable increase in S9.6 positivity, supporting the role of DDX41 in preventing R-loop accumulation (Figure S5A). This prompted us to examine whether ATR kinase inhibition affected R-loop formation, thereby indirectly affecting inflammatory responses. We observed a basal increase in R-loops in ATR kinase inhibitor-treated cells and an enhancement in RNA:DNA hybrids after MEF2A depletion (Figure S5B). These data indicate that R-loops accumulation and inflammatory responses can be uncoupled by deletion of DDX41.

An array of post-translational DDX41 modifications contribute to its nucleic acid-binding capacity, including phosphorylation at Y414 by Bruton's tyrosine kinase (BTK).[13] Having demonstrated the genetic requirement for DDX41 in STING activation following MEF2A depletion, we asked whether chemical inhibition of BTK could abrogate this inflammatory response in U937 cells. Differentiation of U937 cells into monocytes by PMA treatment can promote basal BTK activity (Figure S6A). Like cardiomyocytes, depletion of MEF2A in differentiated U937 cells induces IRF3 and STAT phosphorylation (Figure S6A) and IFN secretion (Figure S6B). Inhibition of BTK kinase activity with ibrutinib significantly reduced phosphorylation of IRF3 and STAT1 relative to vehicle-treated cells in which MEF2A was depleted (Figure S6C). This decrease in IFN responses was not due to changes in the expression of either cGAS or DDX41 (Figure S6C). These data indicate that both the expression of DDX41 and its activation are required for the induction of STING-mediated inflammation in the context of MEF2A silencing. Importantly, the unscheduled activation of these responses could be targeted using chemical kinase inhibitors.

We conducted genome-wide transcriptional profiling to better understanding the mechanisms by which the MEF2A/DDX41 axis promotes inflammatory responses. Overall, the cellular response to MEF2A KD was diminished in DDX41 KO cells relative to WT counterparts (Figure 6D; Data S2). The number of DE genes was also lower in DDX41 KO cells (Figure 6E). Gene set enrichment analysis (GSEA) revealed that DDX41 expression is necessary for the accumulation of genes involved in cytosolic DNA sensing, IFN responses, and antiviral control (Figure 6F). Indeed, an overview of the overlap of genes induced by MEF2A KD identified 1356 DE genes uniquely induced by *MEF2A* silencing in WT, but not KO, cells that were associated with antiviral and IFN responses (Figure 6H). We then conducted functional enrichment analysis on the 418 DE genes induced by loss of MEF2A in both WT and KO cells (263 transcripts) and uniquely DE in *DDX41* KO cells (155 transcripts). These genes were associated with Gene Ontology (GO) biological functions such as cellular differentiation and motility as well as the positive regulation of transcription (Figure 6I). Similar enrichment of transcriptional regulatory pathways was observed using the REACTOME pathway database (Figure 6J). Cellular hyperproliferation and increases in transcription can promote the accumulation of R-loops.[56] As R-loop formation occurs during transcription as the nascent RNA binds back to the DNA template,[6,56] we asked whether the inhibition of de novo transcription could prevent R-loop accumulation after *MEF2A* depletion. Treatment of cells with actinomycin D treatment resulted in decreased S9.6 reactivity in *MEF2A*-depleted cells (Figure 6K). Together, these data suggest that MEF2A maintains the cellular transcriptional output and that its loss promotes unscheduled R-loop accumulation. Moreover, our study shows that these structures likely trigger ATR-dependent, DDX41-/cGAS-dependent activation to promote unscheduled inflammatory responses.

DISCUSSION

In this study, we have identified MEF2A as a regulator of genomic stability that suppresses aberrant STING-dependent IFN activation. The inflammatory response correlated with chromosomal breaks, as evidenced by micronuclei accumulation, increases in γH2A.X, and enhanced phosphorylation of the ATR substrate RPA32. Importantly, inhibition of ATR kinase activity mitigated the induction of IFN responses upon MEF2A depletion. Downregulation of MEF2A expression resulted in the accumulation of R-loops, triple-stranded structures composed of a single-stranded DNA (ssDNA) and an RNA:DNA hybrid. Genetic ablation of *DDX41* or chemical inhibition of the DDX41 regulatory kinase BTK prevented the spontaneous production of IFN that follows the loss of MEF2A. These findings position the transcription factor MEF2A as an enforcer of genomic stability that, when compromised, leads to stress-induced, IFN-mediated inflammation. We found that the acute loss of MEF2A results in the induction an antiviral state across multiple cell types, including cardiomyocytes, fibroblasts, and monocytes. Importantly, understanding the context in which nucleic acid mis-localization and lesion accumulation drives PRR activation is critical for the design and implementation of STING immunomodulatory therapies to manage autoinflammation and cancer.[57]

Depletion of MEF2A expression induced both type I and type III IFN expression. Although these two IFN families promote an antiviral state in target cells, expression of type I and

III IFN receptors varies across tissue types. The type I IFN receptor is expressed on all nucleated cells, while type III IFN receptor expression is restricted primarily to epithelial barriers and a subset of immune cells.[58] We used orthogonal approaches to demonstrate that cardiac muscle cells respond primarily to type I IFNs. Treatment of cells with recombinant type III IFN failed to induce the expression of ISGs, while blockade of secreted type I IFN by treatment with B18R was sufficient to abrogate the induction of antiviral responses induced by the loss of transcriptional homeostasis. The translational potential of our findings is underscored by emerging virus outbreaks, which have refocused attention on the use of recombinant IFN therapies for the clinical management of viral disease.[59] Our findings suggest that type I IFN-targeted therapies may have a greater benefit in the management of cardiotropic virus infections. Conversely, type III IFN induction might contribute less to adverse outcomes after myocardial infarction compared with type I IFN. In addition, induction of IFN responses during ischemic injury to cardiomyocytes can induce STING-/IRF3-dependent inflammation that hinders tissue repair.[33,60]

MEF2 proteins are transcriptional factors implicated in the control of inflammatory responses. In primary aged murine microglial cells, a decrease of MEF2C exacerbated IFN-related inflammatory responses.[29] *In vitro*, microglial expression of MEF2D is required to sustain *Irf7* expression, thereby promoting type I IFN responses.[26] In murine macrophages, MEF2A is necessary to promote chromatin accessibility at the *Ifnb1* locus. Deletion of *Mef2a* suppresses the induction of *Ifnb1* following lipopolysaccharide (LPS) stimulation.[27] Whether MEF2 transcription factors regulate inflammatory responses in human cells is less understood. Our results using immortalized cardiomyocytes, fibroblasts, and myeloid cells indicate that MEF2A acts indirectly as a negative regulator of inflammation by preventing cellular transcriptional stress. Silencing of MEF2A led to the induction of DDRs, as well as the accumulation of R-loops. Previous studies have demonstrated that murine MEF2A silencing can alter the expression profile of cell-cycle regulatory genes, impacting the DNA content profile.[61] Indeed, we observed a downregulation in mitotic regulatory genes upon transient depletion of these genes in human cardiac muscle cells. Importantly, our study correlates the induction of cellular transcriptional stress and IFN-mediated inflammation. Future studies should address the extent to which disruption of the rate cell-cycle progression and transcriptional homeostasis through the loss of transcription factor expression and function promotes inflammatory responses and how these prevent further genomic instability.

R-loops function to promote mitochondrial DNA replication, control transcriptional rates, coordinate faithful chromosome segregation, and facilitate immunoglobulin class-switch recombination.[23,62,63] Pathological R-loop accumulation is the hallmark of inflammatory neurodegenerative diseases such as amyotrophic lateral sclerosis (ALS), fragile X syndrome, and AGS.[7,64] Excessive R-loop formation is also observed in several proliferative malignancies. Cellular nucleases and helicases metabolize RNA:DNA hybrids to mitigate the cytotoxicity of their aberrant accumulation. The expression of Senataxin (SETX) and the related DEAxQ-like domain containing helicase Aquarius (AQR)[53,65] is necessary to curb R-loop accumulation. DEAD/DEAH-box helicases, such as DDX5, DDX19, and DDX41, among others, are also recruited to R-loops and metabolize RNA:DNA hybrids.[9] On the other hand, DExD/H-box helicases, such as DHX9, both promote physiological

R-loop formation at centromeres and drive their pathogenic accumulation during defective splicing.[66] Given the physiological importance of these helicases in the formation and resolution of R-loops, understanding the factors that control their recruitment, activation, and downstream effector functions of these helicases should be further explored across cell and tissue types.

DDX41 can bind both viral dsDNA and viral RNA:DNA hybrids to drive STING-mediated IFN production. In addition, proximity ligation studies show that DDX41 occupancy at R-loops is necessary for their resolution.[15,54] LOF mutations in DDX41 are associated with ineffective hematopoiesis and inherited myelodysplastic syndromes (MDSs).[67] Transgenic zebrafish models show that *ddx41* loss drives R-loop accumulation, which can trigger cGAS-STING pathway-dependent activation of inflammation.[15,55] In this model, ddx41 LOF disrupts splicing of cell-cycle genes and can drive the activation of ATM- and ATR-coordinated DDRs that inhibit erythropoiesis. We found that in the context of acute MEF2A depletion, cGAS, but not IFI16, coordinated the induction of downstream inflammatory responses. Our study demonstrates an expanded role for DDX41 in supporting inflammatory responses, as the accumulation of R-loops induces DDX41-dependent activation of STING and type I IFN-mediated inflammation. However, depletion of either DDX41 or cGAS did not result in a complete abrogation of responses. It is possible that the accumulation of RNA:DNA substrates or DNA breaks in *MEF2A*-deficient cardiac muscle cells could trigger PRR independently or trigger a cGAS-/STING-independent inflammatory pathway.[18]

The accumulation of transcriptional and mitotic R-loops has been shown to trigger ATR activation. ATR localizes to R-loops during mitosis to promote faithful chromosome segregation,[23] and activation of the ATR/Chk1 pathway upon replication stress is important for the recruitment of nucleases into R-loops.[25] The loss of the splicing factor SRSF1 can promote R-loop accumulation and ATR activation.[24,54] Similarly, the disruption of DDX41 expression can enhance R-loop abundance and subsequently activate ATR.[54] Leveraging the MEF2A-depletion model, we showed that ATR kinase activity is necessary to coordinate the induction of DDX41-/cGAS-dependent inflammatory responses upon increased R-loop abundance. Future studies will be crucial to gaining a better understanding of whether ATR promotes the recruitment and activation of RNA:DNA nucleases, such as DDX41, to R-loops to promote resolution, maintain genomic integrity, and drive inflammation.

Overall, this study bridges the activation of the transcriptional stress upon loss of MEF2A with DDX41-dependent activation of STING-mediated inflammation. Specifically, we demonstrate that ATR kinase activity is necessary for the activation of STING activation following R-loop accumulation. As such, our findings reveal a role for MEF2A in the regulation of cellular homeostasis and suggest a potential benefit for the use of specific ATR kinase inhibitors to mitigate deleterious inflammation in neurodegenerative and proliferative diseases defined by increases in R-loop abundance.

Limitations of the study

In this study. we have described the acute effects of MEF2A depletion on the accumulation of R-loops, DDRs, and innate immune inflammation. Our studies were limited to 24 h, which revealed a specific requirement for ATR kinase in the activation of STING. Although

we found ATM and DNA-PK to be dispensable, it is possible that the accrual of R-loop-mediated DNA double-stranded breaks (DSBs) could result in the activation of inflammation by these DRR effectors at later time points. Previous reports show that the loss of DDX41 leads to the concomitant induction of ATR and ATM kinase activity in zebrafish.[55] Future studies are necessary to define whether ATR-dependent IFN production has a role in preventing the accumulation of DSBs and the amplification of inflammation triggered by ATM[47] or DNA-Pk[18,19] during chronic transcriptional stress. Although we demonstrate that DDX41 expression is required for STING activation, the mechanisms for DDX41-dependent immunomodulation remain unknown. Beyond its role in R-loop resolution and cGAS regulation,[12] DDX41 coordinates RNA splicing[68] and processing of ribosomal RNA in hematopoietic and leukemic cells.[67,69] Thus, it is possible that a loss of efficient RNA maturation and protein translation hinders STING activation in non-hematopoietic DDX41-deficient cells. Overall, we have provided evidence to further connect the accumulation of R-loops with ATR activation and inflammation[16] and reveal a need to further investigate the crosstalk between the ATR and DDX41 axis in the maintenance of genomic integrity and the establishment of inflammatory disease.

STAR★METHODS

RESOURCE AVAILABILITY

Lead contact—Further information and requests for resources and reagents should be directed to and will be fulfilled by the lead contact, Adriana Forero (Adriana.forero@osumc.edu).

Materials availability—Plasmids generated in this study are available from the lead contact as determined by Materials Transfer Agreement.

Data and code availability

- The data generated in this study are available via the following accession identifiers on the NCBI-GEO database (GEO: GSE209601). The data used for gene expression analyses described in this manuscript were obtained from the GTEx Portal.
- This paper does not report original code.
- Any additional information required to reanalyze the data reported in this work paper is available from the lead contact upon request.

EXPERIMENTAL MODEL AND STUDY PARTICIPANT DETAILS

Cell lines, cell culture conditions and treatments—Human cardiomyocyte (AC16) and derivate cell lines were grown in Dulbecco's modified Eagle's medium (DMEM) supplemented with 12.5% FBS, 2mM Glutamine, 100 U/ml Penicillin and 100 mg/mL Streptomycin and maintained at 37°C in 5% CO_2. Non-targeted (H1), IRF3, STING, cGAS, IFI16 and DDX41-deficient AC16 cells were generated by CRISPR-Cas9 genome editing as previously described.[77] Transduced cells were enriched using antibiotic selection. BJ/TERT human fibroblasts were cultured in DMEM supplemented with 10% FBS, 2mM

glutamine, 100 U/ml penicillin and 100 mg/mL streptomycin and maintained at 37°C in 5% CO_2. Huh7 human hepatoma cells and derivatives cell lines were cultured in DMEM supplemented with 10% FBS, 2mM Glutamine, 100 U/ml Penicillin and 100 mg/mL Streptomycin and maintained at 37°C in 5% CO_2. U937 monocytes were cultured in RPMI 1640 media supplemented with 10% FBS, 2mM glutamine, 100 U/ml penicillin and 100 mg/mL streptomycin and maintained at 37°C in 5% CO_2. THP-1 monocytes were maintained in RPMI 1640 media supplemented with 10% FBS, 2mM glutamine, 100 U/ml penicillin, 100 mg/mL streptomycin, 1 mM sodium pyruvate, 10 mM HEPES and 0.05 mM 2-mercaptoethanol and maintained at 37°C in 5% CO_2. U937 and THP-1 cells were differentiated for 48 h (h) in their respective complete media containing 40 nM phorbol 12-myristate 13-acetate (PMA) followed by resting for 24 h in RPMI 1640 supplemented with 1% FBS.

Cells were stimulated with recombinant IFNβ (PBL Assay Science) and IFNλ3 (R&D Systems) at the indicated concentrations. Specific kinase inhibitors targeting, ATR (ETP-46465, AZD6738) (Cayman Chemicals), ATM (KU-55933) (SelleckChem), and DNA-PK (NU7441) (SelleckChem) were used at the indicated concentrations. Recombinant B18R (Life Technologies) was used at 1 μg/ml. Etoposide and thapsigargin (Millipore Sigma) were used as indicated. Poly(deoxyadenylic-deoxythymidylic (polydA:dT) was transfected at 1 μg/mL and host immune responses were measured after 24h. Actinomycin D treatment (0.5 μg/mL) was conducted 2h prior to fixation and immunostaining of AC16 cells transfected with either NC or *MEF2A*-targeting dsiRNA.

Viral models—VSV-GFP stock was a gift from Dr. Michael Gale Jr (University of Washington).[70] Sendai Virus (Cantell strain) was acquired from Charles River. AC16 cells were seeded in 24-well plates at a density of 2×10^5 cells/well and transfected with negative control or MEF2A-targeting dsiRNA (IDT). Cells were infected with VSV-GFP at a multiplicity of infection (MOI) of 0.1, consistent with previous reports.[77] Following 24 h of infection, the culture medium was removed, cells were fixed with 4% PFA in PBS, and stained with Crystal violet stain (3% w/v) in 50% ethanol. Plates were imaged using the ChemiDoc XRS+ (BioRad) imaging system. Coxsackievirus B3 (CVB3)-Nancy infectious clone was a kind gift from Dr. Raul Andino (University of California San Francisco). Viral stocks were prepared by linearizing the plasmid by restriction digestion ClaI and *in vitro* transcribing viral RNA. The RNA was transfected into HeLa cells using Mirus X2 and cell supernatants (P0 stocks) were harvested. This supernatant was amplified in HeLa cells to generate P1 stocks that were quantified by plaque assay.[71] AC16 cells were seeded in 12-well plates at a density of 3.5×10^5 cells/well and transfected with negative control or *MEF2A*-targeting dsiRNA. After 24 h, cells were infected with CVB3 (MOI = 5) in a minimal volume for 1h at 37°C in 5% CO2 followed by washing with PBS and culturing in full serum media for 24 h. CVB3 RNA quantification was conducted via SYBR green based qPCR using primers specific to CVB3 VP1.

METHOD DETAILS

Plasmids and oligonucleotides—CRISPR-Cas9 plasmids; pRRL-H1-PURO (non-targeting), pRRL-STING-PURO, pRRL-cGAS-PURO, pRRL-IRF3-PURO, pRRL-IFI16-

PURO were a gift from Dr. Daniel Stetson (University of Washington).[72] The ISRE reporter plasmid, pISRE-sfGFP, was a gift from Dr. Nicholas Heaton (Duke University) and has been previously described.[49] pRRL-DDX41-PURO was generated by cloning single-guide RNA (sgRNA) targeting DDX41 (5′-CCTCATCTTCCGCCTCGGAG-3′) into empty pRRL-Cas9-PURO plasmids as previously described.[72,77] pEGFP-RNASEH1 was a gift from Andrew Jackson & Martin Reijns (Addgene plasmid # 108699). Gene silencing was conducted using dicer-substrate interfering RNA (dsiRNA) specific to *MEF2A, MEF2C, MEF2D, TMEM173, MAVS, IRF1, STAT1* or non-targeting control. Transfection were carried out using 20 nM of dsiRNAs delivered intracellularly using TransIT-TKO (Mirus) according to manufacturer's guidelines. Additional *MEF2A* targeting was done using silencer siRNA (Dharmacon) or scramble control.

RNA extraction and quantification of gene expression—Total RNA was extracted using the NucleoSpin RNA extraction kit (Macherey-Nagel) as indicated by manufacturer guidelines. cDNA synthesis was performed using the QuantiTect RT kit (QIAGEN) or iScript cDNA synthesis kit (BioRad) according to the manufacturer guidelines. Relative quantification of mRNA was done by qPCR using the ViiA7 qPCR system with TaqMan reagents (Life Technologies) or CFX-384 with SSO Advanced Probes reagents (BioRad) using the *HPRT1* as reference gene. Primers and probes used for qPCR assays in this study were acquired from IDT or Life Technologies as indicated.

Western blot analysis—Whole cell lysates were prepared from cells using RIPA buffer (10 mM Tris-Cl (pH 8.0), 1 mM EDTA, 0.5 mM EGTA, 1% Triton X-100, 0.1% sodium deoxycholate, 0.1% SDS, 140 mM NaCl) supplemented with Halt protease and phosphatase inhibitor cocktail (Pierce). Protein quantification and normalization was done using the BCA Protein Assay Kit (Pierce). 10–30 μg total protein were resolved by SDS-PAGE and transferred to PVDF membranes (Bio-Rad). Primary antibody incubations were done overnight with antibodies diluted in 3% BSA in TBS-T (Tris-buffered saline/Tween 20), and species-specific HRP conjugated secondary antibodies. Chemiluminescent image acquisition was performed using a ChemiDoc Touch (BioRad).

RNA sequencing, data processing, and analysis—AC16 cells were seeded in 24-well plates at a density of 2×10^5 cells/well and transfected with either negative control or *MEF2A*-targeting dsiRNA in triplicate. Total RNA was extracted 24 h post transfection as described above. Total RNA fluorometric quantification of was done using the Qubit RNA BR assay kit (Invitrogen) and assessment of RNA integrity was performed using the RNA 6000 Nano Kit in the 2100 Bioanalyzer (Agilent). Library preparation, QC, and sequencing was carried out by Seattle Genomics. Briefly, the synthesis of cDNA libraries was conducted using the TruSeq Stranded mRNA Library Prep Kit. Libraries were sequenced using the Ilumina NextSeq 500 sequencer. Human genome sequence (fasta) and gene transfer files (gtf) were obtained through iGenomes (https://support.illumina.com/sequencing/sequencing_software/igenome.html). Raw RNaseq data (Fastq files) were demultiplexed prior to read quality determination (FastQC, version 0.11.3). Remaining ribosomal RNA reads were digitally removed using Bowtie2 (version 2.3.4). All samples had a minimum of twenty million reads per sample which were aligned

to the human genome (GRCh37) using STAR (version 2.5.3a) and gene counts were derived using HTSeq (version 0.6.1). Library preparation, QC and sequencing of H1 and *DDX41* KO cells mRNA was done by Genewiz (Azenta Life Sciences). Gene counts were filtered (mean of ≥ 10 or greater across all samples) prior to statistical analysis using R statistical programming language (version 3.4.3) and 'edgeR' (version 3.20.9). Gene counts normalization was performed with voom and differential expression analysis was carried out with 'limma' (version 3.34.8). Gene Ontology analysis of differentially expressed transcripts (lfc |0.26|; p value <0.01) was performed using EnrichR.

Micronuclei quantification assay—3×10^6 AC16 cells were plated in a 100-mm dish and treated with 100 ng/mL of nocodazole for 6h. Mitotic cells were harvested by shake-off and washed 3x with PBS. Mitotic cells were then counted and plated in on poly-L-ornithine (PLO)-coated #1.5 12 mm glass-coverslips (Thomas Scientific). Simultaneously, untreated AC16s were plated on PLO-coated coverslips and transfected with 40 nM of non-targeting dsiRNA or dsiRNA targeting *MEF2A* for 24 h. Cells were fixed with 4% Paraformaldehyde for 15 min at room temperature. Fixed cells were then washed 2 times with PBS and blocked in PBS containing 3% BSA and 0.3% Triton X-100. Cells were stained using Lamin B1 antibodies (CST) at 1:200 dilution for 1h at room temperature in PBS containing 1% BSA and 0.1% Triton X-100. Cells were washed 3 times and stained with Alexa 488 conjugated anti-rabbit secondary (Invitrogen) and DAPI (Thermo Scientific) for 1h at room temperature (RT) in PBS containing 1% BSA and 0.1% Triton X-100. Cells were washed and mounted with ProLong Glass Antifade mounting medium (Thermo Fisher). Samples were imaged using a Nikon Eclipse Ti laser scanning confocal microscope, 60x oil-immersion lens. Percent micronuclei was quantified by counting the number of micronuclei per nucleus in the field of view using FIJI.[74]

***In vivo* and *in vitro* R-loop quantification assay—**RNA:DNA hybrid microscopy was conducted as previously described with some modifications.[78] AC16 cells were seeded at 0.5 × 105 cells/well on poly-L-ornithine (PLO)-coated #1.5 12 mm glass-coverslips (Thomas Scientific) and transfected with 40 nM of siNC or siMEF2A for 24 h. Cells were fixed as described above. Fixed cells were then washed 2 times with PBS and blocked in PBS containing 3% BSA and 0.3% Triton X-100. Cells were immunostained using S9.6 antibody (Kerafast) at 1:500 dilution for 1h at RT in PBS containing 1% BSA and 0.1% Triton X-100. Cells were washed 3 times and stained with Alexa 488 conjugated anti-mouse secondary (Invitrogen) and DAPI (Thermo Scientific) for 1h at room temperature in PBS containing 1% BSA and 0.1% Triton X-100. Cells were washed and mounted with ProLong Glass Antifade Mountant (Thermo Fisher). Samples were imaged using a Nikon Eclipse Ti laser scanning confocal microscope, 60x oil-immersion lens. Images were quantified using CellProfiler[79] and presented as mean S9.6 foci intensity per nuclei.

RNA:DNA hybrid dot blots were performed as previously described.[54] In brief, total *MEF2A*-targeted and control cell DNA was extracted using NucleoSpin Tissue DNA kit (Machery-Nagel). DNA was digested with RNase III (Thermo Fisher Scientific) 1U/μg of DNA for 2h at 37°C followed by heat inactivation at 65°C for 20 min. Samples were then split in half and digested with RNaseH (Thermo Fisher Scientific) at 37°C overnight. RNAse

treated DNA was then blotted on nitrocellulose membranes and UV-crosslinked using 1200 μJ × 100 cm^2. Membranes were blocked for 30 min in 3% BSA in TBS and 0.1% Tween 20. Membranes were probed overnight at 4°C with anti-RNA:DNA hybrid (S9.6) (Kerafast) at 1:2,000 dilution or dsDNA antibody (Abcam) at 1:2000 dilution. Membranes were incubated for 45 min with anti-mouse IgG HRP conjugated secondary antibodies for 45 min. Membranes were imaged using Bio-Rad Chemidoc.

ISGF3 Gaussia luciferase and ISRE GFP reporter assays—To generate the ISGF3 Gaussia Luciferase (Gluc) reporter construct, pTRIPZ-5xISGF3-BS-hGLuc-PEST, 5 tandem ISGF3 consensus sequences (5′-CGAAGAAATGAAACT-3′)[80] were cloned with hGLuc-MODC-PEST into a pTRIPZ lentiviral plasmid. Lentivirus encoding the reporter was packaged used to transduce human hepatoma Huh7 cells prior to single-cell cloning of reporter cells. To assess the presence of secreted IFN from dsiRNA transduced AC16 cells, cell supernatants from *MEF2*-depleted and non-targeting control were harvested 24 h post transfection and transferred onto 5xISGF3-GLuc Huh7 reporter cells. Reporter cells were then incubated at 37°C and 5% CO_2 for 24 h prior to assessment of Gaussia luciferase secretion into the media. Sample supernatants were diluted 1:1 with Gaussia Luciferase glow assay substrate (Thermo Fisher Scientific) and luminescence measured using a Synergy HTX (BioTek). To generate ISRE-GFP reporter cell lines, AC16 were stably transduced with lentivirus pISRE-sfGFP and pools were treated with 100IU/ml of recombinant IFNβ or transfected with non-targeting control or *MEF2A*-targeting dsiRNA in the presence of the indicated inhibitors prior to epifluorescent imaging using an EVOS cell imaging system (Thermo Fisher Scientific). For flow cytometric assessment of fluorescence expression, cells were recovered by trypsinization, labeled with Fixable Viability Dye eFluor 780 (Invitrogen) per manufacturer's guidelines and fixed with 4% methanol-free PFA. Fluorescence intensity was using a CANTO analyzer (BD). Flow cytometry data was analyzed using FlowJo (TreeStar).

ELISA quantification of 2′,3′-cGAMP production—H1 control AC16 cardiomyocytes and cGAS KO AC16s were seeded in 12-well plates and transfected with 5 μg of CT-DNA using Transit X2 (Mirus) at a 2:1 ratio for 8 h prior to harvest. Wild-type AC16 cells were seeded in 12-well plates prior to depletion of *MEF2A* with dsiRNA or non-targeting control as described above for 24 h prior to harvest. 2′,3′-cyclic GMP-AMP (cGAMP) was quantified using the Direct 2′,3′-cGAMP ELISA Kit (Arbor Assays) according to manufactures protocol. Briefly, cells were lysed in 150ul of sample diluent solution for 15 min at room temperature. Cell lysates were recovered by scrapping and cell debris was removed by centrifugation at 700 × g at 4°C. Absorbance was read at 450 nm using a Synergy HTX (BioTek).

QUANTIFICATION AND STATISTICAL ANALYSIS

Statistical analysis was performed using GraphPad Prism 9.0 (GraphPad software La Jolla, CA). Statistical significance was calculated as indicated for each experiment in the figure legends and across all experiments, p values of <0.05 were considered significant and are indicated by asterisks (*). The number (N) of technical or biological replicates or individual cells and nuclei are indicated by data points in figures and/or descriptions in figure legends.

Standard deviations (SD) or Standard Error of the Mean (SEM) are reported in figure legends.

Supplementary Material

Refer to Web version on PubMed Central for supplementary material.

ACKNOWLEDGMENTS

We thank Daniel B. Stetson and Haitao Wen for sharing reagents and Richard Robinson and Eugene Oltz for manuscript feedback. This work was supported in part by the Award for Advancing Research in Infection and Immunity (A.F.) and the National Institutes of Health under grant numbers P30 CA016058 (The Ohio State University Comprehensive Cancer Center), R21AI141823 (R.S.), T32AI106677–6 (J.R.S.), and T32HL007312 (A.F.). The content is solely the responsibility of the authors and does not necessarily represent the funding agency views.

INCLUSION AND DIVERSITY

We support inclusive, diverse, and equitable conduct of research.

REFERENCES

1. Chemudupati M, Kenney AD, Bonifati S, Zani A, McMichael TM, Wu L, and Yount JS (2019). From APOBEC to ZAP: Diverse mechanisms used by cellular restriction factors to inhibit virus infections. Biochim. Biophys. Acta Mol. Cell Res. 1866, 382–394. 10.1016/j.bbamcr.2018.09.012. [PubMed: 30290238]
2. Crow YJ, and Manel N (2015). Aicardi–Goutières syndrome and the type I interferonopathies. Nat. Rev. Immunol. 15, 429–440. 10.1038/nri3850. [PubMed: 26052098]
3. Harding SM, Benci JL, Irianto J, Discher DE, Minn AJ, and Greenberg RA (2017). Mitotic progression following DNA damage enables pattern recognition within micronuclei. Nature 548, 466–470. 10.1038/nature23470. [PubMed: 28759889]
4. Mackenzie KJ, Carroll P, Martin C-A, Murina O, Fluteau A, Simpson DJ, Olova N, Sutcliffe H, Rainger JK, Leitch A, et al. (2017). cGAS surveillance of micronuclei links genome instability to innate immunity. Nature 548, 461–465. 10.1038/nature23449. [PubMed: 28738408]
5. Dunphy G, Flannery SM, Almine JF, Connolly DJ, Paulus C, Jønsson KL, Jakobsen MR, Nevels MM, Bowie AG, and Unterholzner L (2018). Non-canonical Activation of the DNA Sensing Adaptor STING by ATM and IFI16 Mediates NF-kB Signaling after Nuclear DNA Damage. Mol. Cell 71, 745–760.e5. 10.1016/j.molcel.2018.07.034. [PubMed: 30193098]
6. Brickner JR, Garzon JL, and Cimprich KA (2022). Walking a tight-rope: The complex balancing act of R-loops in genome stability. Mol. Cell 82, 2267–2297. 10.1016/j.molcel.2022.04.014. [PubMed: 35508167]
7. Cristini A, Tellier M, Constantinescu F, Accalai C, Albulescu LO, Heiringhoff R, Bery N, Sordet O, Murphy S, and Gromak N (2022). RNase H2, mutated in Aicardi-Goutières syndrome, resolves co-transcriptional R-loops to prevent DNA breaks and inflammation. Nat. Commun. 13, 2961. 10.1038/s41467-022-30604-0. [PubMed: 35618715]
8. Crow YJ, Shetty J, and Livingston JH (2020). Treatments in Aicardi–Goutières syndrome. Dev. Med. Child Neurol. 62, 42–47. 10.1111/dmcn.14268. [PubMed: 31175662]
9. Cargill M, Venkataraman R, and Lee S (2021). DEAD-Box RNA Helicases and Genome Stability. Genes 12, 1471. 10.3390/genes12101471. [PubMed: 34680866]
10. Andrisani O, Liu Q, Kehn P, Leitner WW, Moon K, Vazquez-Maldonado N, Fingerman I, and Gale M (2022). Biological functions of DEAD/DEAH-box RNA helicases in health and disease. Nat. Immunol. 23, 354–357. 10.1038/s41590-022-01149-7. [PubMed: 35194205]

11. Zhang Z, Yuan B, Bao M, Lu N, Kim T, and Liu Y-J (2011). The helicase DDX41 senses intracellular DNA mediated by the adaptor STING in dendritic cells. Nat. Immunol. 12, 959–965. 10.1038/ni.2091. [PubMed: 21892174]
12. Singh RS, Vidhyasagar V, Yang S, Arna AB, Yadav M, Aggarwal A, Aguilera AN, Shinriki S, Bhanumathy KK, Pandey K, et al. (2022). DDX41 is required for cGAS-STING activation against DNA virus infection. Cell Rep. 39, 110856. 10.1016/j.celrep.2022.110856. [PubMed: 35613581]
13. Lee K-G, Kim SS-Y, Kui L, Voon DC-C, Mauduit M, Bist P, Bi X, Pereira NA, Liu C, Sukumaran B, et al. (2015). Bruton's Tyrosine Kinase Phosphorylates DDX41 and Activates Its Binding of dsDNA and STING to Initiate Type 1 Interferon Response. Cell Rep. 10, 1055–1065. 10.1016/j.celrep.2015.01.039. [PubMed: 25704810]
14. Stavrou S, Aguilera AN, Blouch K, and Ross SR (2018). DDX41 Recognizes RNA/DNA Retroviral Reverse Transcripts and Is Critical for In Vivo Control of Murine Leukemia Virus Infection. mBio 9, 009233–18. 10.1128/mBio.00923-18.
15. Weinreb JT, Ghazale N, Pradhan K, Gupta V, Potts KS, Tricomi B, Daniels NJ, Padgett RA, De Oliveira S, Verma A, and Bowman TV (2021). Excessive R-loops trigger an inflammatory cascade leading to increased HSPC production. Dev. Cell 56, 627–640.e5. 10.1016/j.devcel.2021.02.006. [PubMed: 33651979]
16. Forero A, Giacobbi NS, McCormick KD, Gjoerup OV, Bakkenist CJ, Pipas JM, and Sarkar SN (2014). Simian Virus 40 Large T Antigen Induces IFN-Stimulated Genes through ATR Kinase. J. Immunol. 192, 5933–5942. 10.4049/jimmunol.1303470. [PubMed: 24799566]
17. Blackford AN, and Jackson SP (2017). ATM, ATR, and DNA-PK: The Trinity at the Heart of the DNA Damage Response. Mol. Cell 66, 801–817. 10.1016/j.molcel.2017.05.015. [PubMed: 28622525]
18. Burleigh K, Maltbaek JH, Cambier S, Green R, Gale M, James RC, and Stetson DB (2020). Human DNA-PK activates a STING-independent DNA sensing pathway. Sci. Immunol. 5, eaba4219. 10.1126/sciimmunol.aba4219. [PubMed: 31980485]
19. Ferguson BJ, Mansur DS, Peters NE, Ren H, and Smith GL (2012). DNA-PK is a DNA sensor for IRF-3-dependent innate immunity. Elife 1, e00047. 10.7554/eLife.00047. [PubMed: 23251783]
20. Justice JL, and Cristea IM (2022). Nuclear antiviral innate responses at the intersection of DNA sensing and DNA repair. Trends Microbiol. 30, 1056–1071. 10.1016/j.tim.2022.05.004. [PubMed: 35641341]
21. Ragu S, Matos-Rodrigues G, and Lopez BS (2020). Replication Stress, DNA Damage, Inflammatory Cytokines and Innate Immune Response. Genes 11, 409. 10.3390/genes11040409. [PubMed: 32283785]
22. Saldivar JC, Cortez D, and Cimprich KA (2017). The essential kinase ATR: ensuring faithful duplication of a challenging genome. Nat. Rev. Mol. Cell Biol. 18, 622–636. 10.1038/nrm.2017.67. [PubMed: 28811666]
23. Kabeche L, Nguyen HD, Buisson R, and Zou L (2018). A mitosis-specific and R loop–driven ATR pathway promotes faithful chromosome segregation. Science 359, 108–114. 10.1126/science.aan6490. [PubMed: 29170278]
24. Matos DA, Zhang J-M, Ouyang J, Nguyen HD, Genois M-M, and Zou L (2020). ATR Protects the Genome against R Loops through a MUS81-Triggered Feedback Loop. Mol. Cell 77, 514–527.e4. 10.1016/j.molcel.2019.10.010. [PubMed: 31708417]
25. Hodroj D, Recolin B, Serhal K, Martinez S, Tsanov N, Abou Merhi R, and Maiorano D (2017). An ATR-dependent function for the Ddx19 RNA helicase in nuclear R-loop metabolism. EMBO J. 36, 1182–1198. 10.15252/embj.201695131. [PubMed: 28314779]
26. Lu F, Wang R, Xia L, Nie T, Gao F, Yang S, Huang L, Shao K, Liu J, and Yang Q (2021). Regulation of IFN-Is by MEF2D Promotes Inflammatory Homeostasis in Microglia. JIR 14, 2851–2863. 10.2147/JIR.S307624.
27. Cilenti F, Barbiera G, Caronni N, Iodice D, Montaldo E, Barresi S, Lusito E, Cuzzola V, Vittoria FM, Mezzanzanica L, et al. (2021). A PGE2-MEF2A axis enables context-dependent control of inflammatory gene expression. Immunity 0. 10.1016/j.immuni.2021.05.016.

28. Xue F, Tian J, Yu C, Du H, and Guo L (2021). Type I interferon response-related microglial Mef2c deregulation at the onset of Alzheimer's pathology in 53FAD mice. Neurobiol. Dis. 152, 105272. 10.1016/j.nbd.2021.105272. [PubMed: 33540048]
29. Deczkowska A, Matcovitch-Natan O, Tsitsou-Kampeli A, Ben-Hamo S, Dvir-Szternfeld R, Spinrad A, Singer O, David E, Winter DR, Smith LK, et al. (2017). Mef2C restrains microglial inflammatory response and is lost in brain ageing in an IFN-I-dependent manner. Nat. Commun. 8, 717. 10.1038/s41467-017-00769-0. [PubMed: 28959042]
30. Chen X, Gao B, Ponnusamy M, Lin Z, and Liu J (2017). MEF2 signaling and human diseases. Oncotarget 8, 112152–112165. 10.18632/oncotarget.22899. [PubMed: 29340119]
31. Lin Q, Schwarz J, Bucana C, and Olson EN (1997). Control of Mouse Cardiac Morphogenesis and Myogenesis by Transcription Factor MEF2C. Science 276, 1404–1407. 10.1126/science.276.5317.1404. [PubMed: 9162005]
32. Naya FJ, Black BL, Wu H, Bassel-Duby R, Richardson JA, Hill JA, and Olson EN (2002). Mitochondrial deficiency and cardiac sudden death in mice lacking the MEF2A transcription factor. Nat. Med. 8, 1303–1309. 10.1038/nm789. [PubMed: 12379849]
33. King KR, Aguirre AD, Ye Y-X, Sun Y, Roh JD, Ng RP, Kohler RH, Arlauckas SP, Iwamoto Y, Savol A, et al. (2017). IRF3 and type I interferons fuel a fatal response to myocardial infarction. Nat. Med. 23, 1481–1487. 10.1038/nm.4428. [PubMed: 29106401]
34. Majidi SP, Reddy NC, Moore MJ, Chen H, Yamada T, Andzelm MM, Cherry TJ, Hu LS, Greenberg ME, and Bonni A (2019). Chromatin Environment and Cellular Context Specify Compensatory Activity of Paralogous MEF2 Transcription Factors. Cell Rep. 29, 2001–2015.e5. 10.1016/j.celrep.2019.10.033. [PubMed: 31722213]
35. Soveg FW, Schwerk J, Gokhale NS, Cerosaletti K, Smith JR, Pairo-Castineira E, Kell AM, Forero A, Zaver SA, Esser-Nobis K, et al. (2021). Endomembrane targeting of human OAS1 p46 augments antiviral activity. Elife 10, e71047. 10.7554/eLife.71047. [PubMed: 34342578]
36. Kessler DS, Levy DE, and Darnell JE (1988). Two interferon-induced nuclear factors bind a single promoter element in interferon-stimulated genes. Proc. Natl. Acad. Sci. USA 85, 8521–8525. 10.1073/pnas.85.22.8521. [PubMed: 2460869]
37. Symons JA, Alcamí A, and Smith GL (1995). Vaccinia virus encodes a soluble type I interferon receptor of novel structure and broad species specificity. Cell 81, 551–560. 10.1016/0092-8674(95)90076-4. [PubMed: 7758109]
38. Miyamoto M, Fujita T, Kimura Y, Maruyama M, Harada H, Sudo Y, Miyata T, and Taniguchi T (1988). Regulated expression of a gene encoding a nuclear factor, IRF-1, that specifically binds to IFN-β gene regulatory elements. Cell 54, 903–913. 10.1016/S0092-8674(88)91307-4. [PubMed: 3409321]
39. Suschak JJ, Wang S, Fitzgerald KA, and Lu S (2016). A cGAS-Independent STING/IRF7 Pathway Mediates the Immunogenicity of DNA Vaccines. J. Immunol. 196, 310–316. 10.4049/jimmunol.1501836. [PubMed: 26590319]
40. Ablasser A, and Hur S (2020). Regulation of cGAS- and RLR-mediated immunity to nucleic acids. Nat. Immunol. 21, 17–29. 10.1038/s41590-019-0556-1. [PubMed: 31819255]
41. Saito T, Owen DM, Jiang F, Marcotrigiano J, and Gale M (2008). Innate immunity induced by composition-dependent RIG-I recognition of hepatitis C virus RNA. Nature 454, 523–527. 10.1038/nature07106. [PubMed: 18548002]
42. Ishikawa H, Ma Z, and Barber GN (2009). STING regulates intracellular DNA-mediated, type I interferon-dependent innate immunity. Nature 461, 788–792. 10.1038/nature08476. [PubMed: 19776740]
43. Yount JS, Gitlin L, Moran TM, and López CB (2008). MDA5 Participates in the Detection of Paramyxovirus Infection and Is Essential for the Early Activation of Dendritic Cells in Response to Sendai Virus Defective Interfering Particles. J. Immunol. 180, 4910–4918. 10.4049/jimmunol.180.7.4910. [PubMed: 18354215]
44. Liu S, Cai X, Wu J, Cong Q, Chen X, Li T, Du F, Ren J, Wu Y-T, Grishin NV, and Chen ZJ (2015). Phosphorylation of innate immune adaptor proteins MAVS, STING, and TRIF induces IRF3 activation. Science 347, aaa2630. 10.1126/science.aaa2630. [PubMed: 25636800]

45. Petrasek J, Iracheta-Vellve A, Csak T, Satishchandran A, Kodys K, Kurt-Jones EA, Fitzgerald KA, and Szabo G (2013). STING-IRF3 pathway links endoplasmic reticulum stress with hepatocyte apoptosis in early alcoholic liver disease. Proc. Natl. Acad. Sci. USA 110, 16544–16549. 10.1073/pnas.1308331110. [PubMed: 24052526]
46. Chen H, Wang G, Chen L, Dai B, Yu F, Qian H, Shao C, Zhang X, Hu J, Li H, et al. (2018). The Augmented R-Loop Is a Unifying Mechanism for Myelodysplastic Syndromes Induced by High-Risk Splicing Factor Mutations. Mol. Cell 8, 412–425. 10.1016/j.molcel.2017.12.029.
47. Härtlova A, Erttmann SF, Raffi FA, Schmalz AM, Resch U, Anugula S, Lienenklaus S, Nilsson LM, Kröger A, Nilsson JA, et al. (2015). DNA Damage Primes the Type I Interferon System via the Cytosolic DNA Sensor STING to Promote Anti-Microbial Innate Immunity. Immunity 42, 332–343. 10.1016/j.immuni.2015.01.012. [PubMed: 25692705]
48. Maréchal A, and Zou L (2013). DNA Damage Sensing by the ATM and ATR Kinases. Cold Spring Harbor Perspect. Biol. 5, a012716. 10.1101/cshperspect.a012716.
49. Froggatt HM, Harding AT, Chaparian RR, and Heaton NS (2021). ETV7 limits antiviral gene expression and control of influenza viruses. Sci. Signal. 14, eabe1194. 10.1126/scisignal.abe1194. [PubMed: 34257104]
50. Bianchi V, Pontis E, and Reichard P (1986). Changes of deoxyribonucleoside triphosphate pools induced by hydroxyurea and their relation to DNA synthesis. J. Biol. Chem. 261, 16037–16042. [PubMed: 3536919]
51. Stork CT, Bocek M, Crossley MP, Sollier J, Sanz LA, Chédin F, Swigut T, and Cimprich KA (2016). Co-transcriptional R-loops are the main cause of estrogen-induced DNA damage. Elife 5, e17548. 10.7554/eLife.17548. [PubMed: 27552054]
52. Crossley MP, Bocek M, and Cimprich KA (2019). R-Loops as Cellular Regulators and Genomic Threats. Mol. Cell 73, 398–411. 10.1016/j.molcel.2019.01.024. [PubMed: 30735654]
53. Nguyen HD, Yadav T, Giri S, Saez B, Graubert TA, and Zou L (2017). Functions of Replication Protein A as a Sensor of R Loops and a Regulator of RNaseH1. Mol. Cell 65, 832–847.e4. 10.1016/j.molcel.2017.01.029. [PubMed: 28257700]
54. Mosler T, Conte F, Longo GMC, Mikicic I, Kreim N, Möckel MM, Petrosino G, Flach J, Barau J, Luke B, et al. (2021). R-loop proximity proteomics identifies a role of DDX41 in transcription-associated genomic instability. Nat. Commun. 12, 7314. 10.1038/s41467-021-27530-y. [PubMed: 34916496]
55. Weinreb JT, Gupta V, Sharvit E, Weil R, and Bowman TV (2022). Ddx41 inhibition of DNA damage signaling permits erythroid progenitor expansion in zebrafish. Haematologica 107, 644–654. 10.3324/haematol.2020.257246. [PubMed: 33763998]
56. Kotsantis P, Silva LM, Irmscher S, Jones RM, Folkes L, Gromak N, and Petermann E (2016). Increased global transcription activity as a mechanism of replication stress in cancer. Nat. Commun. 7, 13087. 10.1038/ncomms13087. [PubMed: 27725641]
57. Decout A, Katz JD, Venkatraman S, and Ablasser A (2021). The cGAS–STING pathway as a therapeutic target in inflammatory diseases. Nat. Rev. Immunol. 21, 548–569. 10.1038/s41577-021-00524-z. [PubMed: 33833439]
58. Dowling JW, and Forero A (2022). Beyond Good and Evil: Molecular Mechanisms of Type I and III IFN Functions. J. Immunol. 208, 247–256. 10.4049/jimmunol.2100707. [PubMed: 35017214]
59. Beyer DK, and Forero A (2022). Mechanisms of Antiviral Immune Evasion of SARS-CoV-2. J. Mol. Biol. 434, 167265. 10.1016/j.jmb.2021.167265. [PubMed: 34562466]
60. Calcagno DM, Ng RP, Toomu A, Zhang C, Huang K, Aguirre AD, Weissleder R, Daniels LB, Fu Z, and King KR (2020). The myeloid type I interferon response to myocardial infarction begins in bone marrow and is regulated by Nrf2-activated macrophages. Sci. Immunol. 5, eaaz1974. 10.1126/sciimmunol.aaz1974. [PubMed: 32978242]
61. Desjardins CA, and Naya FJ (2017). Antagonistic regulation of cell-cycle and differentiation gene programs in neonatal cardiomyocytes by homologous MEF2 transcription factors. J. Biol. Chem. 292, 10613–10629. 10.1074/jbc.M117.776153. [PubMed: 28473466]
62. Yu K, Chedin F, Hsieh C-L, Wilson TE, and Lieber MR (2003). R-loops at immunoglobulin class switch regions in the chromosomes of stimulated B cells. Nat. Immunol. 4, 442–451. 10.1038/ni919. [PubMed: 12679812]

63. Aguilera A, and Gómez-González B (2017). DNA–RNA hybrids: the risks of DNA breakage during transcription. Nat. Struct. Mol. Biol. 24, 439–443. 10.1038/nsmb.3395. [PubMed: 28471430]
64. Park K, Ryoo J, Jeong H, Kim M, Lee S, Hwang S-Y, Ahn J, Kim D, Moon HC, Baek D, et al. (2021). Aicardi-Goutières syndrome-associated gene SAMHD1 preserves genome integrity by preventing R-loop formation at transcription–replication conflict regions. PLoS Genet. 17, e1009523. 10.1371/journal.pgen.1009523. [PubMed: 33857133]
65. Sollier J, Stork CT, García-Rubio ML, Paulsen RD, Aguilera A, and Cimprich KA (2014). Transcription-Coupled Nucleotide Excision Repair Factors Promote R-Loop-Induced Genome Instability. Mol. Cell 56, 777–785. 10.1016/j.molcel.2014.10.020. [PubMed: 25435140]
66. Chakraborty P, Huang JTJ, and Hiom K (2018). DHX9 helicase promotes R-loop formation in cells with impaired RNA splicing. Nat. Commun. 9, 4346. 10.1038/s41467-018-06677-1. [PubMed: 30341290]
67. Chlon TM, Stepanchick E, Hershberger CE, Daniels NJ, Hueneman KM, Kuenzi Davis A, Choi K, Zheng Y, Gurnari C, Haferlach T, et al. (2021). Germline DDX41 mutations cause ineffective hematopoiesis and myelodysplasia. Cell Stem Cell 28, 1966–1981.e6. 10.1016/j.stem.2021.08.004. [PubMed: 34473945]
68. Ma J, Mahmud N, Bosland MC, and Ross SR (2022). DDX41 is needed for pre- and postnatal hematopoietic stem cell differentiation in mice. Stem Cell Rep. 17, 879–893. 10.1016/j.stemcr.2022.02.010.
69. Kadono M, Kanai A, Nagamachi A, Shinriki S, Kawata J, Iwato K, Kyo T, Oshima K, Yokoyama A, Kawamura T, et al. (2016). Biological implications of somatic DDX41 p.R525H mutation in acute myeloid leukemia. Exp. Hematol. 44, 745–754.e4. 10.1016/j.exphem.2016.04.017. [PubMed: 27174803]
70. Fredericksen BL, and Gale M (2006). West Nile Virus Evades Activationof Interferon Regulatory Factor 3 through RIG-I-Dependent and -Independent Pathways without Antagonizing Host Defense Signaling. J. Virol. 80, 2913–2923. 10.1128/JVI.80.6.2913-2923.2006. [PubMed: 16501100]
71. Laufman O, Perrino J, and Andino R (2019). Viral Generated Inter-Organelle Contacts Redirect Lipid Flux for Genome Replication. Cell 178, 275–289.e16. 10.1016/j.cell.2019.05.030. [PubMed: 31204099]
72. Gray EE, Winship D, Snyder JM, Child SJ, Geballe AP, and Stetson DB (2016). The AIM2-like Receptors Are Dispensable for the Interferon Response to Intracellular DNA. Immunity 45, 255–266. 10.1016/j.immuni.2016.06.015. [PubMed: 27496731]
73. Schwerk J, Soveg FW, Ryan AP, Thomas KR, Hatfield LD, Ozarkar S, Forero A, Kell AM, Roby JA, So L, et al. (2019). RNA-binding protein isoforms ZAP-S and ZAP-L have distinct antiviral and immune resolution functions. Nat. Immunol. 20, 1610–1620. 10.1038/s41590-019-0527-6. [PubMed: 31740798]
74. Schindelin J, Arganda-Carreras I, Frise E, Kaynig V, Longair M, Pietzsch T, Preibisch S, Rueden C, Saalfeld S, Schmid B, et al. (2012). Fiji: an open-source platform for biological-image analysis. Nat. Methods 9, 676–682. 10.1038/nmeth.2019. [PubMed: 22743772]
75. Stirling DR, Swain-Bowden MJ, Lucas AM, Carpenter AE, Cimini BA, and Goodman A (2021). CellProfiler 4: Improvements in speed, utility, and usability. BMC Bioinformatics 22, 433. 10.1186/s12859-021-04344-9.2. [PubMed: 34507520]
76. Chen EY, Tan CM, Kou Y, Duan Q, Wang Z, Meirelles GV, Clark NR, and Ma'ayan A (2013). Enrichr: Interactive and collaborative HTML5 gene list enrichment analysis tool. BMC Bioinformatics 14, 128. 10.1186/1471-2105-14-128.3. [PubMed: 23586463]
77. Forero A, Ozarkar S, Li H, Lee CH, Hemann EA, Nadjsombati MS, Hendricks MR, So L, Green R, Roy CN, et al. (2019). Differential Activation of the Transcription Factor IRF1 Underlies the Distinct Immune Responses Elicited by Type I and Type III Interferons. Immunity 51, 451–464.e6. 10.1016/j.immuni.2019.07.007. [PubMed: 31471108]
78. Kim D, Liu Y, Oberly S, Freire R, and Smolka MB (2018). ATR-mediated proteome remodeling is a major determinant of homologous recombination capacity in cancer cells. Nucleic Acids Res. 46, 8311–8325. 10.1093/nar/gky625. [PubMed: 30010936]

79. Stirling DR, Swain-Bowden MJ, Lucas AM, Carpenter AE, Cimini BA, and Goodman A (2021). CellProfiler 4: improvements in speed, utility and usability. BMC Bioinf. 22, 433. 10.1186/s12859021-04344-9.

80. Schmid S, Mordstein M, Kochs G, García-Sastre A, and Tenoever BR (2010). Transcription factor redundancy ensures induction of the antiviral state. J. Biol. Chem. 285, 42013–42022. 10.1074/jbc.M110.165936. [PubMed: 20943654]

Highlights

- Loss of MEF2A, not other members of the MEF2 family, promotes STING-dependent inflammation
- MEF2A expression prevents the accumulation of R-loops that induce IFN
- The RNA:DNA helicase, DDX41, and cGAS are necessary for IFN induction
- ATR kinase activity, but not ATM or DNA-PK, is required for STING activation

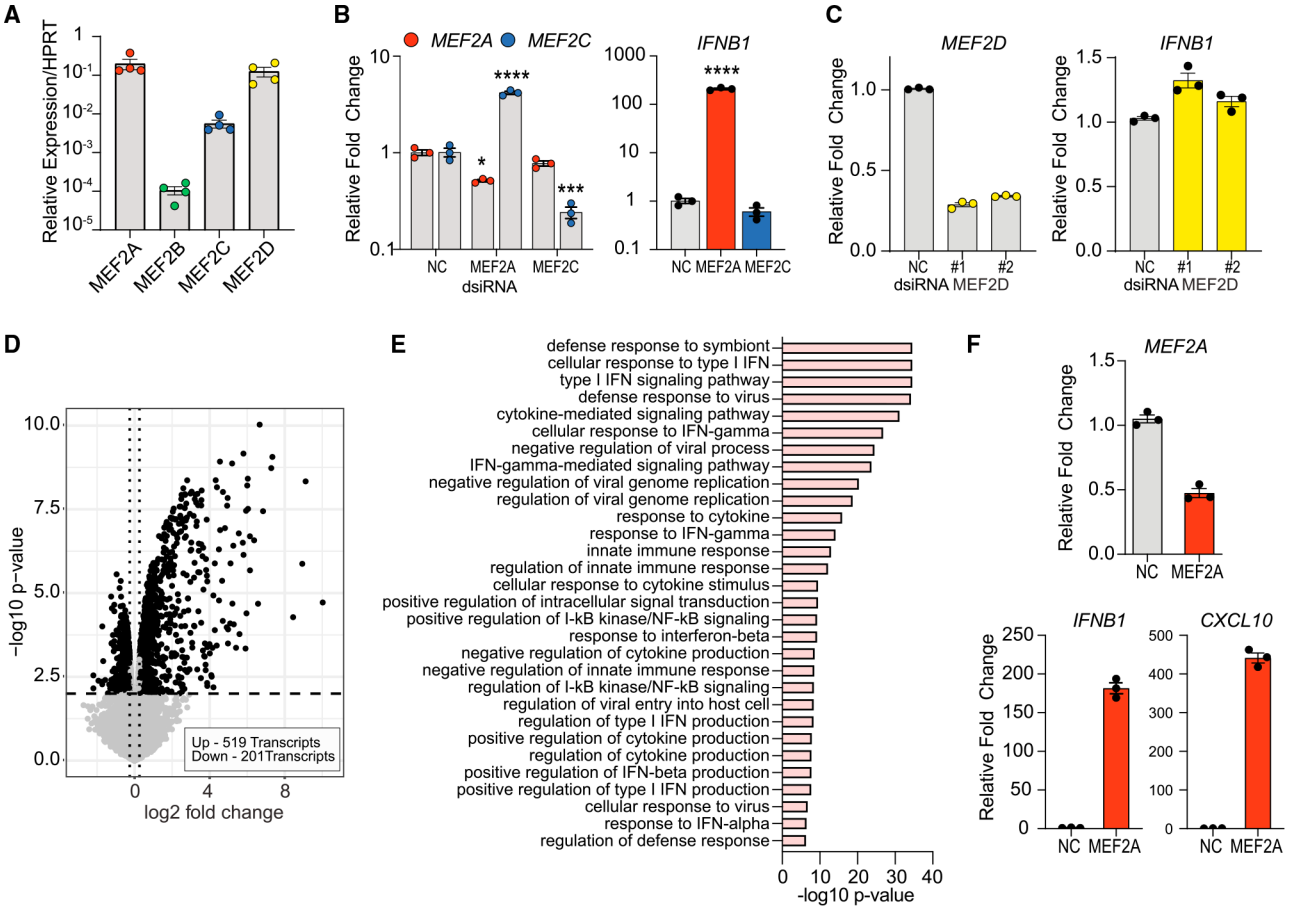

Figure 1. MEF2A silencing induces innate immune inflammation

(A) Expression of MEF2 transcripts was calculated relative to *HPRT1*. Bars represent the average expression across 4 independent experiments, ± SEM.

(B) Bar graphs represent relative expression of *MEF2A* (red) and *MEF2C* (blue) mRNA following dsiRNA transfection (left). Expression of *IFNB1* mRNA following dsiRNA-mediated depletion of *MEF2A* (red) or *MEF2C* (blue). Relative fold change was calculated relative to NC-transfected cells and normalized to *HPRT1* (value1).

(C) Bar graphs represent the average relative expression of *MEF2D* (yellow, left) and *IFNB1* (right) mRNA following transfection of AC16 cells with two distinct dsiRNA targeting MEF2D or NC. Relative fold change in expression was calculated as described above. Experiments represent average of 3 individual experiments. ****p ≤ % 0.0001, ***p ≤ % 0.001, and *p < 0.05 as determined by one-way ANOVA.

(D) Volcano plot of differentially expressed genes (Log2 fold-change [LFC] |0.26|; adjusted [adj] p value = 0.01) following knockdown (KD) of *MEF2A* with dsiRNA. 519 transcripts were significantly upregulated and 201 transcripts were downregulated (black) relative to NC-transfected cells. Each dot represents a unique transcript, and dashed lines indicate threshold of significance. Non-significant changes in gene expression are highlighted in gray. Bar graph represents the top 30 GO biological processes enriched among the genes upregulated by *MEF2A* depletion.

(E) Loss of MEF2A promotes the expression of *IFNB1* and *CXCL10* mRNA. Relative ISG expression was normalized to NC-transfected cells (value of 1) and normalized to *HPRT1*. Data are representative of the average of 3 individual replicates ± SEM.
See also Figure S1 and Data S1.

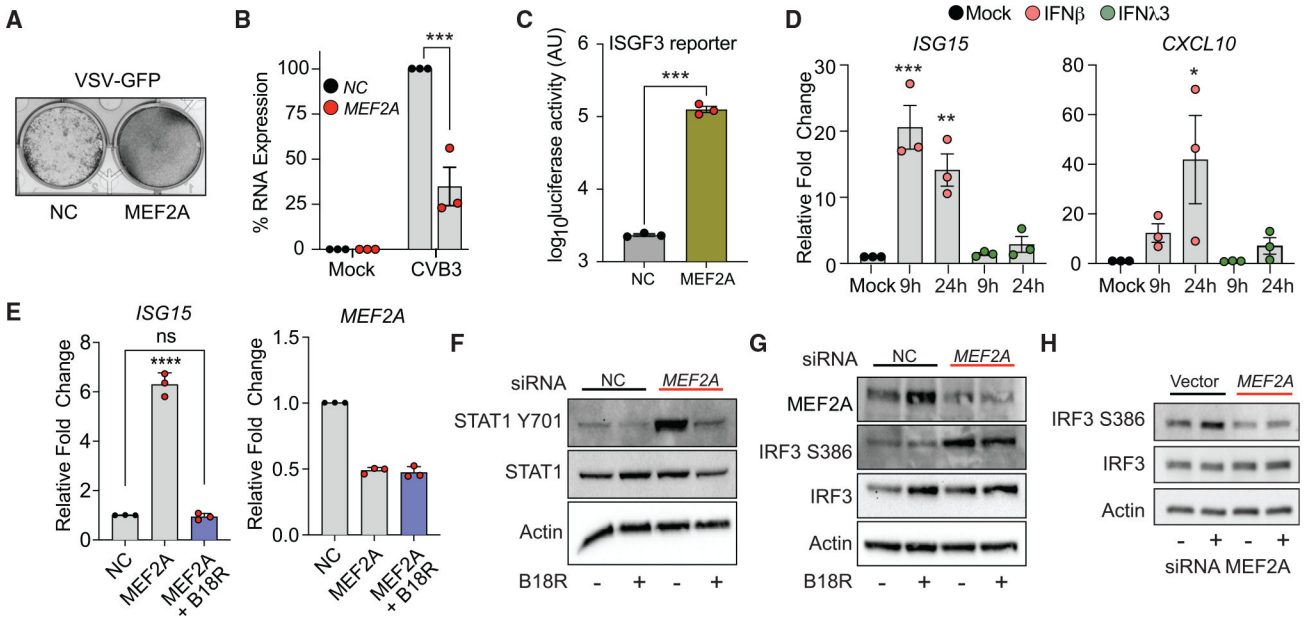

Figure 2. Type I IFN drives antiviral states upon MEF2A loss

(A) Loss of *MEF2A* protects cells against the cytopathic effect of vesicular stomatitis virus (VSV).

(B) *MEF2A* loss protects against Coxsackievirus B (CVB3). Bar graphs represent mean percent reduction of CVB3 viral RNA expression (VP1) in *MEF2A*-depleted cells (red) relative to NC-transfected cells (black) across 3 independent experiments ± SEM.

(C) Bar graphs represent average *Gaussia* luciferase activity from 5xISGF3-Gluc Huh7 reporter cells stimulated with supernatants derived from AC16 cells after *MEF2A* depletion. Data represent 3 independent experiments ± SEM. ***p ≤ % 0.001, as determined by Student's t test.

(D) AC16 cells were stimulated with 25 IU/mL IFNβ (pink) or 100 ng/mL IFNλ3 (green) for the indicated times prior to total RNA harvest. Relative expression of *ISG15* and *CXCL10* mRNA was measured relative to *HPRT1* and normalized to mock-treated cells (value 1). Bar graphs represent average of 3 independent experiments ± SEM. ***p ≤ % 0.001, **p ≤ % 0.01, and *p < 0.05 as determined by two-way ANOVA.

(E) Type I IFN was blocked by pre-treatment of AC16 cells with 1 μg/mL recombinant B18R prior to transfection with dsiRNA. Expression of ISG15 (left) or *MEF2A* (right) mRNA was quantified relative to *HPRT1* and normalized to NC-transfected cells (value of 1). Bar graphs represent average of 3 independent experiments ± SEM, and ****p ≤ % 0.0001 as determined by one-way ANOVA.

(F) Activation of IFN signaling was probed by measuring phosphorylated STAT1 (Y701), STAT1, and Actin protein expression by western blot.

(G) AC16 cells were treated as mentioned above and the levels of phosphorylated IRF3 (S386), IRF3, and Actin were measured by western blot analysis.

(H) Vector control AC16 cells and cells overexpressing MEF2A were transfected with dsiRNA targeting the 3′ UTR of the endogenous *MEF2A*. The levels of phosphorylated IRF3 (S386), IRF3, and Actin were measured by western blot analysis.

See also Figure S2.

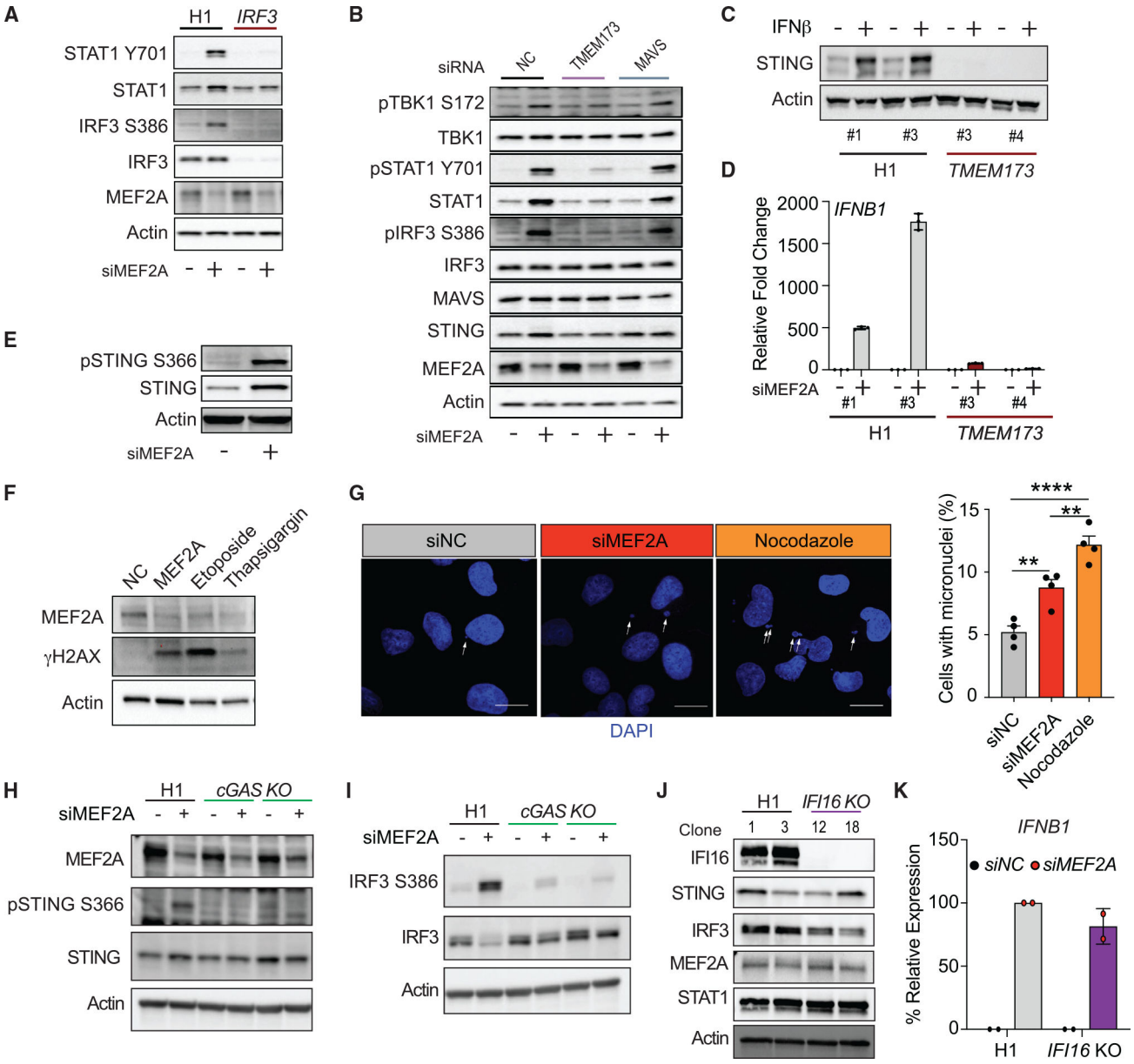

Figure 3. STING expression is necessary for the induction of IFN-mediated inflammation

(A) AC16 cells stably transduced with non-targeting single-guide RNA (sgRNA) (H1) or IRF3-targeting sgRNA (IRF3) were transfected with NC or *MEF2A*-targeting dsiRNA for 24 h. Analysis of protein expression of phosphorylated IRF3 (S386) and STAT1 (Y701), IRF3, STAT1, MEF2A, and Actin protein by western blot.

(B) Signal transduction through STING, but not MAVS, is required for IFN induction after the loss of MEF2A. AC16 cells were transfected with dsiRNA targeting *MAVS, TMEM173* (STING), or NC for 24 h. Cells were transfected with dsiRNA targeting *MEF2A* or NC for an additional 24 h. Whole-cell protein lysates were probed for phosphorylated TBK1 (S172), IRF3 (S386), and STAT1 (Y701), TBK1, STAT1, IRF3, MAVS, STING, MEF2A, and Actin. Western blot representative of 3 independent experiments.

(C) H1 and *TMEM173*-targeted cells were mock treated or stimulated with IFNβ (25 IU/mL) for 24 h, and Actin protein expression was measured by western blot. Numbers indicate clonal cell populations.

(D) AC16 H1 and *TMEM173* (STING) KO cells transfected with dsiRNA targeting *MEF2A*. Bar graphs represent the average relative MEF2A mRNA expression relative to *HPRT1* expression and NC-transfected cells (value 1) across 2 individual experiments ± SEM. Numbers indicate clonal cell lines.

(E) AC16 cells were transfected with NC or MEF2A-targeting siRNA for 24 h. Protein expression analysis for phosphorylated STING (S366), STING, and Actin.

(F) AC16 cells were transfected with either NC or *MEF2A*-target dsiRNA. In parallel, cells were stimulated with etoposide or thapsigargin. 24 h post-treatment, MEF2A, γH2AX, and Actin protein expression was measured by western blot. Images are representative of 3 independent experiments.

(G) Representative micrographs of micronuclei detected by confocal microscopy of DAPI-stained DNA in AC16 cells transfected with NC or *MEF2A*-targeting dsiRNA or cells treated with nocodazole as positive control. Bar graphs represent the percentage of micronuclei-positive cells following NC (gray), *MEF2A* KD (red), or treatment with nocodazole (orange). Data represent average of 4 independent experiments ± SEM. ****$p \leq 0.0001$ and **$p \leq 0.01$ as determined by one-way ANOVA.

(H) AC16 expressing a non-targeting sgRNA (H1) or clones of cells in which cGAS has been targeted (cGAS KO) were transfected with NC or *MEF2A*-targeting dsiRNA. 24 h post-transfection, protein expression of MEF2A, phosphorylated STING (S366), total STING, and Actin was measured.

(I) Expression of phosphorylated IRF3 (S386), total IRF3, and Actin. Western blots are representative of at least 3 independent experiments.

(J) Clonal line IFI16 KOs were derived as indicated by individual numbers, and expression of IFI16, STING, IRF3, MEF2A, STAT1, and Actin was assessed by western blot.

(K) AC16 H1 (clone1) and *IFI16* KO (clone 18) cells were transfected with NC or *MEF2A*-targeting dsiRNA. 24 h post-transfection, relative expression of *IFNB1* mRNA was quantified by qPCR. Bar graphs represent *IFNB1* mRNA expression relative to *HPRT1* and H1 siMEF2A transfection (value 100). Data represent average of independent experiments ± SEM.

See also Figure S3.

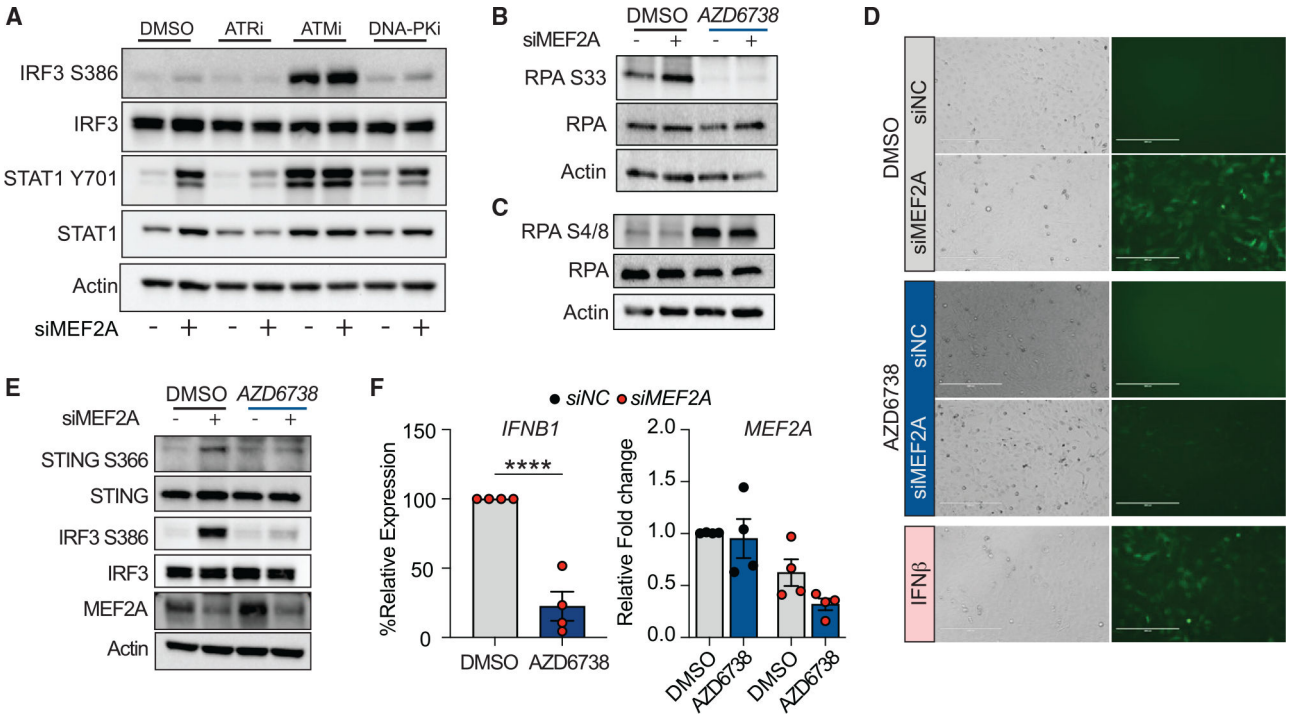

Figure 4. ATR kinase activity is required for IFN induction

(A) Human fibroblast cells, BJ/TERT, were pre-treated with ATR (ETP-46464, 2 μM) ATM (KU-55933, 30 μM), and DNA-PK (NU7441, 4 μM) kinase inhibitors or DMSO as vehicle control for 2 h prior to dsiRNA transfection. Whole-cell lysates were harvested 24 h post-transfection, and phosphorylated IRF3 (S386) and STAT1 (Y701), IRF3, STAT1, and Actin protein expression was measured. Data are representative of 3 independent experiments.

(B) BJ/TERT cells were pre-treated with AZD6738 (2 μM) for 2 h prior to transfection with dsiRNA. Whole-cell lysates were probed for phosphorylated RPA32 (S33), total RPA32, and Actin by western blot.

(C) Phosphorylation of ATM/DNA-Pk substrate RPA32 (S4/8) following *MEF2A* depletion and ATR kinase inhibition as determined by western blot.

(D) AC16 ISRE-GFP reporter cell lines were pre-treated with AZD6738 (2 μM) for 2 h prior to dsiRNA transfection. Control cells were stimulated with 100 IU/mL recombinant IFNβ. Fluorescent signal was detected by epifluorescent microscopy.

(E) AC16 cells were treated as described above. Expression of phosphorylated IRF3 (S386) and STING (S366), STING, IRF3, MEF2A, and Actin was measured by western blot. Data are representative of 3 independent experiments.

(F) Bar graphs represent the percentage of relative expression of endogenous *IFNB1* mRNA expression in transfected AC16 cells in response to ATR kinase inhibition. Relative *IFNB1* mRNA expression was calculated relative to expression in DMSO-treated cells and normalized to HPRT1 control (value 100%). Relative *MEF2A* expression was normalized to *HPRT1* expression and DMSO-treated cells (value 1). Data represent the average of 4 individual experiments ± SEM. ****$p \leq 0.0001$ as determined by Student's t test.

See also Figure S4.

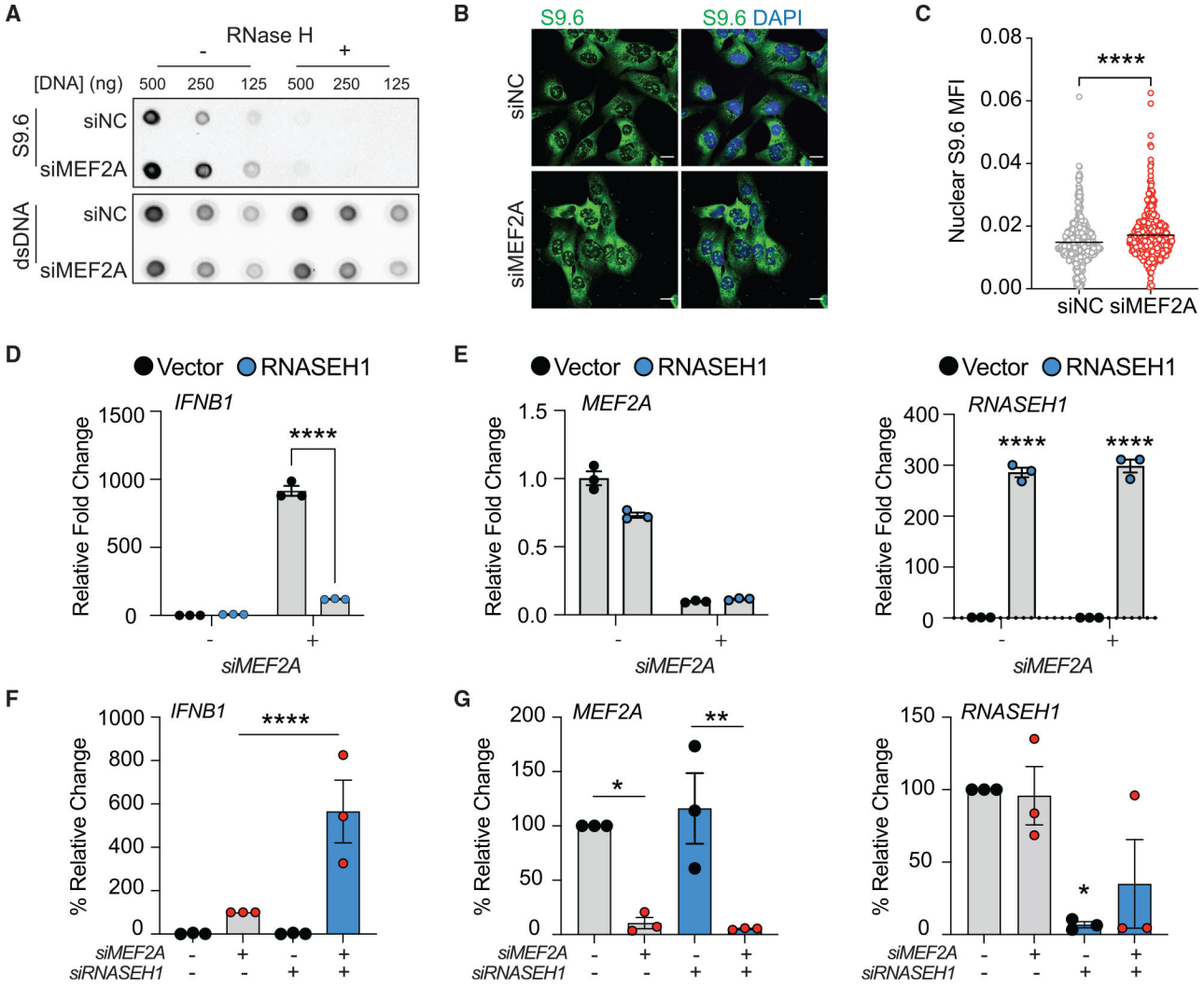

Figure 5. MEF2A depletion promotes R-loop accumulation

(A) RNA:DNA hybrid formation in AC16 cells transfected with NC or *MEF2A*-targeting dsiRNA. Serial dilutions of RNase III-treated nucleic acids were probed with S9.6 antibody or dsDNA-specific antibodies. RNase H treatment was used for RNA:DNA hybrid degradation.

(B) Representative micrograph of S9.6 staining (green) in AC16 cells following dsiRNA transfection. DAPI staining (blue) indicates cell nucleus. Scale bar indicates 20 μM.

(C) Quantification of nuclear S9.6 staining in cells transfected with NC or MEF2A-targeting dsiRNA. Data points represent individual nuclei.

(D) AC16 cells were transfected with *RNASEH1* expression plasmids of empty vector control (vector) overnight followed by dsiRNA transfection. Bar graphs represent the fold change in *IFNB1* mRNA expression relative to vector/NC control and *HPRT1* (relative value of 1) ± SD. ****p ≤ 0.0001 as determined by two-way ANOVA. Data are representative of experiments conducted in triplicate.

(E) Bar graphs represent the average expression of *MEF2A* and *RNASEH1* in transfected cells relative to HPRT1 ± SD. ****p ≤ 0.0001 as determined by two-way ANOVA.

(F) Cells were co-transfected with dsiRNA targeting *MEF2A* and/or *RNASEH1* for 24 h prior to harvesting of total RNA. Bar graphs represent the percent fold change in *IFNB1* mRNA expression relative to *HPRT1* ± SD. Data were normalized to *IFNB1* mRNA expression in *MEF2A:NC* dsiRNA co-transfected cells (relative value of 100%). ****p = 0.0015 as determined by one-way ANOVA. Data are representative of triplicate experiments. (G) Bar graphs represent the average expression of *MEF2A* and *RNASEH1* in transfected cells relative to HPRT1 across triplicate experiments ± SD. *$p \leq 0.05$ and $p \leq 0.05$ as determined by one-way ANOVA.

See also Figure S5.

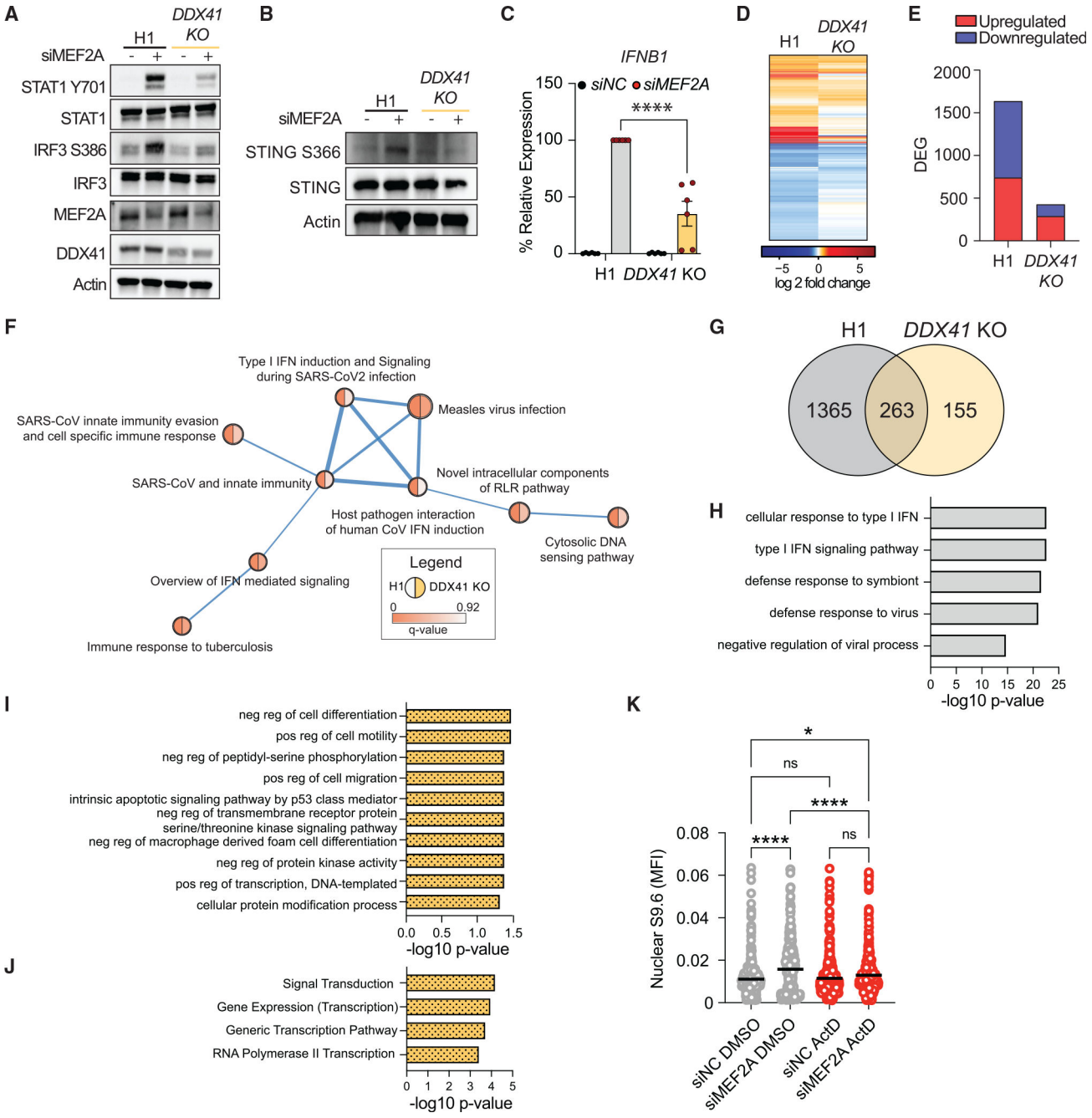

Figure 6. MEF2A depletion triggers DDX41-mediated inflammation and transcriptional stress

(A) AC16 DDX41-deficient cells were generated by CRISPR-Cas9 genome editing (DDX41 KO). WT (H1) and DDX41 KO cells were transfected with NC or MEF2A-targeting dsiRNA for 24 h post-transfection. Whole-cell lysates were probed for protein expression of phosphorylated STAT1 (Y701) and IRF3 (S386), STAT1, IRF3, MEF2A, DDX41 and Actin. Data are representative of a minimum of 3 independent experiments.

(B) Control cells (H1) and DDX41 KO cells were transfected with NC or MEF2A-targeting dsiRNA as indicated above. Phosphorylated STING (S366), STING, DDX41, and Actin protein expression determined by western blot.

(C) AC16 H1 and DDX41 KO cells were transfected with NC or MEF2A-targeting dsiRNA for 24 h prior to harvesting total RNA. Bar graphs represent percentage of IFNB1 mRNA expression relative to HPRT1 control and normalization to IFNB1 mRNA expression in H1 cells transfected with dsiMEF2A (100%). Bar graphs represent average expression across 5 independent experiments ±SEM. ****$p \leq 0.0001$ as determined by two-way ANOVA.
(D) Hierarchical clustering and relative expression of 1,793 differentially expressed genes (LFC |0.26|; adj p value = 0.01) following KD of MEF2A with dsiRNA in either WT (H1) or DDX41 KO cells.
(E) Bar graph represents upregulated (red) and downregulated (blue) genes following MEF2A silencing in each cell type.
(F) The affiliation network represents gene connectivity across 9 GO terms identified by GSEA. Each bubble represents a unique term, with enrichment (adj p value) represented by bubble color for in H1 (left) or DDX41 KO (right) cells. The weighed edges represent transcript overlap.
(G) Venn diagram of overlap of DE genes following *MEF2A* silencing.
(H) GO biological process enrichment analysis of the 1,385 DE genes (DEGs) unique to WT cells.
(I) GO term enrichment analysis of the union of overlapping DEGs across genotypes and DDX41 KO cells. Bar graphs represent the −log10 p value of enrichment for each term.
(J) REACTOME pathway enrichment analysis of the overlap of DEGs across genotypes and DDX41 KO cells. Bar graphs represent the −log10 p value of enrichment for each term.
(K) *In vivo* assessment of RNA:DNA hybrids following *MEF2A* depletion and inhibition of de novo transcription by actinomycin D treatment.
See also Figure S6 and Data S2.

KEY RESOURCES TABLE

REAGENT or RESOURCE	SOURCE	IDENTIFIER
Antibodies		
Donkey Anti-Mouse IgG (HRP-Conjugated)	Jackson ImmunoResearch	RRID: AB_2340770
Donkey Anti-Rabbit IgG (HRP-Conjugated)	Jackson ImmunoResearch	RRID: AB_10015282
b-Actin-HRP (13E5)	Cell Signaling Technology	RRID: AB_1903890
Mouse anti DNA-RNA hybrid [S9.6]	Kerafast	RRID:AB_2687463
Rabbit anti GAPDH (D16H11)	Cell Signaling Technology	RRID:AB_10622025
Rabbit anti cGAS (D1D3G)	Cell Signaling Technology	RRID:AB_2799712
Rabbit anti MEF2A	Bethyl Laboratories	RRID:AB_10954235
Rabbit anti STAT1	Cell Signaling Technology	RRID:AB_2197984
Rabbit anti phosphorylated STAT1 (Y701)	Cell Signaling Technology	RRID:AB_561284
Rabbit anti IRF1 (D5E4)	Cell Signaling Technology	RRID:AB_10949108
Rabbit anti IRF3 (D6I4C)	Cell Signaling Technology	RRID:AB_2722521
Rabbit anti IRF3 (phospho S386) [EPR2346]	Abcam	RRID:AB_1523836
Rabbit anti DDX41	Thermo Scientific	RRID:AB_2809226
Mouse anti IFI16	Santa Cruz Biotechnology	RRID:AB_627775
Rabbit anti phosphorylated STING	Cell Signaling Technology	RRID:AB_2737062
Rabbit anti STING	Cell Signaling Technology	RRID:AB_2799947
Rabbit anti phospho histone H2A.X (Ser139)	Cell Signaling Technology	RRID:AB_2118010
Rabbit anti ATF4 (D4B8)	Cell Signaling Technology	RRID:AB_2616025
Rabbit anti XBP-1s (D2CF1F)	Cell Signaling Technology	RRID:AB_2687943
Rabbit anti phosphorylated CHK1	Cell Signaling Technology	RRID:AB_331212
Rabbit anti phospho RPA32 (S33)	Bethyl Laboratories	RRID:AB_2180847
Rat anti RPA32	Cell Signaling Technology	RRID:AB_2238543
Rabbit anti phospho RPA32 (S4/8)	Bethyl Laboratories	RRID:AB_210547
Bacterial and virus strains		
VSV-GFP	Michael Gale	Fredericksen and Gale, 2006[70]
Coxsackie Virus B3 (Nancy)	Raul Andino	Laufman et al., 2019[71]
Stellar Competent Cells *E. coli* HST08 strain	Takara	Cat# 636763
Chemicals, peptides, and recombinant proteins		
Human recombinant IFNβ	PBL Assay Science	111415–1
Human recombinant IFNλ3	R&D Systems	5259-IL-025
Mirus Bio TransIT-X2	Mirus Bio LLC	MIR6000
Mirus Bio TransIT-TKO	Mirus Bio LLC	MIR2150
DAPI	Thermo Fisher Scientific	D1306
RNase T1	Thermo Fisher Scientific	EN0541
RNase III	Thermo Fisher Scientific	AM2290
RNase H	Thermo Fisher Scientific	AM2292

REAGENT or RESOURCE	SOURCE	IDENTIFIER
B18R	Invitrogen	34–8185-81
Etoposide	Sigma-Aldrich	341205
Thapsigargin	Sigma-Aldrich	T9033
Nocodazole	Sigma-Aldrich	M1404
ATR inhibitor, ETP-46465	Cayman Chemicals	19809
ATR inhibitor, AZD6738	Cayman Chemicals	21035
ATM inhibitor, KU-55933	SelleckChem	S1092
DNA-Pk inhibitor, NU7441	SelleckChem	S26638
Hydroxyurea	Sigma-Aldrich	H8627–1G
100x Halt protease and phosphatase inhibitor	Thermo Fisher Scientific	78420
Ibrutinib	Med Chem Express	PCI-32765
polydA:dT	InVivoGen	tlrl-patn
Actinomycin D	Sigma-Aldrich	A9415
Critical commercial assays		
NucleoSpin RNA II	Macherey-Nagel	740955.250
NucleoSpin Tissue DNA kit	Macherey-Nagel	740952.5
QuantiTect RT kit	QIAGEN	205314
iSCRIPT cDNA Synthesis Kit	Bio-Rad	1708891
SsoAdvanced Universal Probes Supermix	Bio-Rad	1725281
TaqMan Universal Master Mix II, no UNG	Thermo Fisher Scientific	4440048
Qubit RNA BR Assay Kit	Thermo Fisher Scientific	Q10210
Pierce BCA Protein Assay	Thermo Fisher Scientific	PI23227
RNA 6000 Nano Kit	Agilent	5067–1511
2’,3’-Cyclic GAMP ELISA Kit	Arbor Assays	K067-H1
Deposited data		
RNA sequencing data	This paper	GEO: GSE209601
Experimental models: Cell lines		
AC16	Millipore	Cat# SCC109, RRID:CVCL_4U18
BJ/TERT	Saumendra Sarkar	RRID:CVCL_6573
U937	ATCC	Cat# CRL-1593.2, RRID:CVCL_0007
THP-1	ATCC	Cat# TIB-202, RRID:CVCL_0006
Huh7	ATCC	RRID: CVCL_0336
TMEM173 KO AC16	This Paper	N/A
IRF3KO AC16	This Paper	N/A
*cGAS*KO AC16	This Paper	N/A
*IFI16*KO AC16	This Paper	N/A
*DDX41*KO AC16	This Paper	N/A
5xISGF3-GLuc Huh7	This Paper	N/A
pISRE-sfGFP AC16	This Paper	N/A

REAGENT or RESOURCE	SOURCE	IDENTIFIER
Oligonucleotides		
DsiRNA MEF2A	Integrated DNA Technologies	hs.Ri.MEF2A.13.2
DsiRNA MEF2A	Integrated DNA Technologies	hs.Ri.MEF2A.13.1
siRNA MEF2A	Thermo Fisher Scientific	Assay ID 107760
DsiRNA Negative control	Integrated DNA Technologies	51–01-14–04
siRNA Negative control	Thermo Fisher Scientific	AM4613
DsiRNA TMEM173	Integrated DNA Technologies	hs.Ri.TMEM173.13.1
DsiRNA MAVS	Integrated DNA Technologies	hs.Ri.MAVS.13.1
DsiRNA MEF2C	Integrated DNA Technologies	hs.Ri.MEF2C.13.2
DsiRNA MEF2D-1	Integrated DNA Technologies	hs.Ri.MEF2D.13.1
DsiRNA MEF2D-2	Integrated DNA Technologies	hs.Ri.MEF2D.13.2
DsiRNA RNASEH1	Integrated DNA Technologies	hs.Ri.RNASEH1.13.1
siRNA IRF1	Thermo Fisher Scientific	115266
siRNA STAT1	Thermo Fisher Scientific	M-003543–01-0005
MEF2A	Life Technologies	Hs01050406_g1
MEF2B	Integrated DNA Technologies	Hs.PT.58.39043087
MEF2C	Integrated DNA Technologies	Hs.PT.58.14426705
MEF2D	Integrated DNA Technologies	Hs.PT.58.20959128
IFNB1	Integrated DNA Technologies	Hs.PT.58.39481063.g
CXCL10	Thermo Fisher Scientific	Hs00171042_m1
ISG15	Integrated DNA Technologies	Hs.PT.58.39185901.g
HPRT1	Integrated DNA Technologies	Hs.PT.58v.45621572
CVB3 VP1 F: 5’-ACGAATCCCAGTGTGTTTTGG-3’ R:	Integrated DNA technologies	N/A
5’-TGCTCAAAAACGGTATGGACAT-3’		
CHMP2A F: 5’-CGCGAGCGACAGAAACTAGAG-3’ R:	Integrated DNA technologies	N/A
5’ -CCCGCATCAATACAAACTTGC-3’		
5xISGF3_BS-hGLuc_PEST gBLOCK 5’-ATCTCGATC	Integrated DNA technologies	N/A
GAAGAAATGAAACTTGATCATCGCCG AAGAAATGA		
AACTGCGAATCTGACGAAGAAATGAA ACTCGCTTC		
GTAACGAAGAAATGAAACTCGTAGAC TACCGAAGA		
AATGAAACTCCCGGGTAGGGCCCAAT TCGAGTCGA		
GGTAGGCGTGTACGGTGGGAGGTCTAT ATAAGCAG		
AGCTGGTTTAGTGAACCGTCAGATCGC CTGGAGAG		
ATCTTTGTCGATCCTACCATCCACTCG ACACACCCG		

REAGENT or RESOURCE	SOURCE	IDENTIFIER
CCAGCGACCACTGCCAAGCTTCCGAG CTCTCGCTC		
TAGAgccgccaccATGGGAGTCAAAGTTC TGTTTGCCC		
TGATCTGCATCGCTGTGGCCGAGGCC AAGCCCACC		
GAGAACAACGAAGACTTCAACATCGT GGCCGTGGC		
CAGCAACTTCGCGACCACGGATCTCG ATGCTGACC		
GCGGGAAGTTGCCCGGCAAGAAGCTG CCGCTGGA		
GGTGCTCAAAGAGATGGAAGCCAATG CCCGGAAAG		
CTGGCTGCACCAGGGGCTGTCTGATCT GCCTGTCC		
CACATCAAGTGCACGCCCAAGATGAA GAAGTTCATC		
CCAGGACGCTGCCACACCTACGAAGG CGACAAAGA		
GTCCGCACAGGGCGGCATAGGCGAGG CGATCGTC		
GACATTCCTGAGATTCCTGGGTTCAAG GACTTGGAG		
CCCATGGAGCAGTTCATCGCACAGGTC GATCTGTGT		
GTGGACTGCACAACTGGCTGCCTCAA AGGGCTTGC		
CAACGTGCAGTGTTCTGACCTGCTCA AGAAGTGGC		
TGCCGCAACGCTGTGCGACCTTTGCC AGCAAGATC		
CAGGGCCAGGTGGACAAGATCAAGGG GGCCGGTG		
GTGACAAGCTCCCTAGAAGTCATGGAT TCCCACCT		
GCAGTGGCCGCGCAGGACGATGGTAC CCTACCGA		
TGTCTTGCGCTCAAGAGAGCGGAATG GACCGACAT		
CCAGCGGCGTGTGCCTCAGCAAGAAT TAACGT		
TTAG-3’		
5xISGF3_BS GA fwd 5’-ATTTTATTATCTAACTGCTGA	Integrated DNA technologies	N/A
TCGAGTGTAGCCAGATCTCCCGGGATC TCGATCG		
AAGAAATGAAACTTGATCA-3’		
hLuc_PEST GA rev 5’-CTGTATTGCTACTTGTGATTGC	Integrated DNA technologies	N/A
TCCATGTTTTTCTAGGTCTCGAGCTAA ACGTTAATT		
CTTGCTGAGGCACAC-3’		

REAGENT or RESOURCE	SOURCE	IDENTIFIER
RNASEH1 F: 5'-CCTCCAGTTAGCAGAGACACGT-3'	Integrated DNA technologies	N/A
R: 5'-CCAGTAAACGCCGATTCCTGCT-3'		
MEF2A F: 5'-CAAGGGCATGATGCCTCCACTA-3'	Integrated DNA technologies	N/A
R: 5'-GCTGAGTACACAAGTCCTTGCG-3'		
IFNB1 F: 5'-CTTGGATTCCTACAAAGAAGCAGC-3'	Integrated DNA technologies	N/A
R: 5'-TCCTCCTTCTGGAACTGCTGCA-3'		
HPRT1 F: 5'-CATTATGCTGAGGATTTGGAAAGG-3'	Integrated DNA technologies	N/A
R: 5'-CTTGAGCACACAGAGGGCTACA-3'		
Recombinant DNA		
pISRE-sfGFP	Nicholas Heaton	Froggatt et al., 2021[49]
pRRL-H1-PURO	Daniel Stetson	Gray et al., 2015[72]
pRRL-STING-PURO	Daniel Stetson	Gray et al., 2015[72]
pRRL-cGAS-PURO	Daniel Stetson	Gray et al., 2015[72]
pRRL-IRF3-PURO	Ram Savan	Schwerk et al., 2019[73]
pRRL-IFI16-PURO	Daniel Stetson	Gray et al., 2015[72]
pRRL-DDX41-PURO	This paper	N/A
pTRIPZ-5xISGF3_BS-hGLuc_PEST	This paper	N/A
pEGFP-RNASEH1	Addgene	RRID: Adggene_108699
pMEF2A-GFP	This paper	N/A
Software and algorithms		
FIJI	Schindelin et al., 2012[74]	https://imagej.net/software/fiji/
CellProfiler	Stirling et al., 2021[75]	https://cellprofiler.org/
GraphPad Prism 9	GraphPad Software	RRID: SCR_002798
R Studio 1.1.442	Rstudio	RRID: SCR_000432
EnrichR	Chen et al., 2013[76]	RRID: SCR_001575
Partek Flow	Partek	https://www.partek.com/partek-flow/